Pan-genomic analysis shows hemizygous *PTEN* loss tumors are associated with immune evasion and poor outcome

Vidotto T[1]*, Melo CM[1]*, Lautert-Dutra W[1], Chaves LP[1], Reis RB[2], Squire JA[§ 1,3]

**joint first authors*

[1]*Department of Genetics, Medicine School of Ribeirão Preto, University of São Paulo, Ribeirão Preto, Brazil.*

[2] *Division of Urology, Department of Surgery and Anatomy, Medicine School of Ribeirão Preto, University of São Paulo, Ribeirão Preto, Brazil.*

[3] *Department of Pathology and Molecular Medicine, Queen's University, Kingston, Canada.*

§ Corresponding author: Jeremy Andrew Squire. E-mail: jsquireinsp@gmail.com

ABSTRACT

Somatic mutations of the *PTEN* tumor suppressor gene in tumors are associated with advanced disease, chemotherapy resistance, and poor survival. *PTEN* point mutations or deletions that inactivate one (hemizygous loss) or both genes (homozygous loss) are frequent somatic events in all cancers. Mouse models have shown that the tumor-promoting abilities of *Pten* loss can exhibit haploinsufficiency, with hemizygous loss being more tumorigenic than homozygous loss. Most *PTEN* biomarker studies of human tumors have not considered potential differences between hemi- and homozygous loss. To determine the oncogenic role of hemizygous *PTEN* loss in a range of solid tumors, we performed an analysis of 393 (4.03%) to be homozygous and 2292 (23.51%) hemizygous *PTEN* losses derived from 9,748 cases of the Cancer Genome Atlas (TCGA) cohort analyzing 31 tumor types. Both hemi- and homozygous *PTEN* loss were strongly associated with a less favorable outcome and the acquisition of genomic features of tumor progression. Combined survival analysis of the TCGA cohort showed that patients with hemizygous *PTEN* loss had worse outcomes than homozygous loss and *PTEN* intact ($P<0.0001$). Hemizygous loss in tumors of colon, head and neck and cervix had less favorable outcomes compared to homozygous loss and intact tumors. Tumors with hemizygous *PTEN* loss had significantly higher levels of nonsilent mutations, intratumor heterogeneity, aneuploidy, and percent genome altered compared to homozygous loss. These data suggest that the more extensive genomic diversity associated with hemizygous loss could be providing the selective advantage and worse outcome in these tumor types. Transcriptome analysis showed that most investigated tumors had immune-related pathways up- or downregulated when *PTEN* was lost. CIBERSORT analysis found that the imputed immune cell abundances were significantly altered for both types of *PTEN* loss, with changes in head and neck,

cervix, stomach, prostate, brain, and colon being more evident in hemizygous loss tumors. Collectively, these data draw attention to the need for more comprehensive *PTEN* biomarker studies of the prognostic role of hemizygous loss. Future studies should also investigate the role of reduced levels of PTEN protein on differential treatment responses to chemo- or immunotherapy in specific tumor types.

Keywords PanCancer; haploinsufficiency; tumor suppressor gene; mouse model; somatic mutation; tumor microenvironment; genomic instability; gene dosage; immunotherapy; immune evasion; *in silico* analysis

BACKGROUND

The PTEN tumor suppressor functions as a phosphatase, which metabolizes PIP3, the lipid product of PI3-Kinase that antagonizes the activation of the oncogenic PI3K/AKT/mTOR signaling axis [1]. In addition to its role as a primary regulator of the cancer cell growth, recent findings also implicate PTEN in mediating aspects of the immune response against cancer [2].

PTEN is frequently lost, either partially affecting one copy of the gene (hemizygous loss; HemDel) or entirely affecting both copies of the gene (homozygous loss; HomDel), in a range of sporadic tumor types. A variety of mechanisms can cause *PTEN* gene inactivation, including missense and truncation mutations and deletions, as well as reduced expression of active PTEN protein mediated by promoter methylation, the effects of miRNAs, and the suppression of PTEN enzyme activity [3]. Loss of function of the *PTEN* tumor suppressor has been observed as one of the most common events in many types of cancer [4], having the greatest selection pressure for deletion based on an analysis of 746 human cancer genomes [5].

The *Pten* conditional knockout mouse model closely mimics human prostate initiation and progression [6]. Studies showed that loss of one copy of the *Pten* allele dramatically increases the rate of tumors [7]. It was proposed that haploinsufficiency of the *Pten* gene resulted in reduced levels of the functional protein that were insufficient for preventing tumor formation. Similar studies using a brain-tumor-specific model also showed that *Pten* haploinsufficiency accelerated the formation of glioblastomas [8]. Analysis of hypomorphic *Pten* mice demonstrated that as little as a 20% reduction of PTEN protein contributed to the development of prostate cancer in mice [9]. These and other mouse studies [10] show that minor reductions in PTEN protein levels can profoundly influence tumorigenesis [11]. The findings from *Pten* murine tumor models are consistent with the precise cellular controls needed to regulate *PTEN* stability and function [12], implying that even subtle changes in *PTEN* expression may have profound effects on cancer development and progression [3].

Álvarez-Garcia et al. [13] recently surveyed the solid tumor literature on *PTEN* loss resulting from a mutation within the coding region of the gene; hemizygous or homozygous deletions of the gene as assessed by loss of heterozygosity (LOH), reduced copy number in array CGH analysis or loss of *PTEN* by FISH. The majority of tumor-associated missense mutations resulted in a loss or significantly reduced phosphatase activity or protein truncations. *PTEN* was found to demonstrate distinct patterns of somatic mutation leading to loss of function across different tumor types. The majority of glioblastomas display loss of function of *PTEN* in agreement with data from TCGA showing *PTEN* deletions in 143/170 (85%) of glioblastomas [14]. Other human tumor types found to have frequent *PTEN* deletions and/or loss of protein are cancers of prostate (25-50%), endometrium (50%), ovarian (30-50%), lung (35-55%), breast (30-40%) and colon (10-40%) [15]. Moreover, it was found that single copy inactivation of

PTEN was far more common than mutation or deletion of both copies [13]. The PI3K/AKT/mTOR consortium study further suggested that partial copy number *PTEN* loss was associated with less favourable outcome than complete loss across all available TCGA data [16]. These data, together with the murine *Pten* studies of tumorigenesis, formed the rationale for this PanCancer study that aimed to address the idea that partial loss of function of *PTEN* by hemizygous loss may confer a greater selective advantage for a subset of tumors than complete loss of function by homozygous loss (reviewed in [17]).

Our previous study examining the genomic impact of *PTEN* loss using TCGA data demonstrated that primary prostate tumors harboring *PTEN* deletions had enhanced levels of aneuploidy and non-synonymous mutations [18]. However, it was unclear whether the genomic instability generated by loss of one copy of *PTEN* was associated with tumor progression. Other studies examining the impact of *PTEN* loss using TCGA and other public domain datasets do not distinguish between one copy loss and complete loss of the gene [19–22]. Similarly, most *PTEN* cancer biomarker studies using immunohistochemistry and fluorescence *in situ* hybridization (FISH) have not been rigorously standardized [13,15,23,24]. For these reasons, the impact of partial loss of function due to one copy loss of *PTEN* is unknown for most cancers.

This study analyzed the TCGA data comparing oncogenic and immunophenotypic features that distinguish hemizygous *PTEN* loss from homozygous loss across the PanCancer cohort. Our analysis also examines the relationships between *PTEN* intact, hemi-, and homozygous loss with tumor progression and disease outcome.

METHODS

Data download and processing

We initially downloaded raw and level 3 PanCancer normalized RNAseq, array-CGH, and SNV from 10,713 samples derived from 31 tumor types from The Cancer Genome Atlas (TCGA) cohort (www.gdc.cancer.gov). These initial cases were used to determine outcome, genomic alterations and relative immune abundances. For the differential gene expression analysis (DEG) cBioPortal had 9,748 cases were available from primary tumors as described in Supplementary table 1.

Raw RNAseq experiments were performed through Illumina HiSeq 2000 RNA Sequencing platform. Copy number data were obtained from array-CGH experiments performed with the Affymetrix Genome-Wide Human SNP Array 6.0. DNA sequencing was performed in Illumina Genome Analyzer DNA sequencing. Clinical data for progression-free interval and overall survival were obtained for all patients from the TCGA cohort. Raw RNAseq data of all investigated tumors were downloaded through *TCGAbiolinks* package in R [25]. All analyses were conducted with data derived from primary tumors.

Defining *PTEN* deletions

PTEN deletions were characterized by using GISTIC-derived categorical somatic copy number alterations (SCNA). In brief, GISTIC identifies a cutoff for copy number loss or gain using the log2 continuous data form each individual segments, such as genes and other regions [26]. These analyses were performed by the TCGA group for the PanCancer analysis. We obtained, for our study, the Level 3 copy number calls for *PTEN* gene resulting from whole genome detection of copy number changes or point mutations inactivating either one or both copies of the gene [18]. The calls were defined as HomDel (two copies with loss/mutation), HemDel (one copy loss or mutation), intact *PTEN* (both copies present without mutation) and duplications of the *PTEN* gene [27].

PTEN duplications consisted of the presence of gain of an extra copy of the entire gene or regions at 10q23.31 that included *PTEN*.

Gene expression and enrichment analyses.

Analysis of gene expression was performed on the RNAseq level. Raw read counts for TCGA-tumors were downloaded using FANTOM-CAT/recount2 (https://jhubiostatistics.shinyapps.io/recount/) [28,29]. The subset of samples was compiled using each patient's clinical information, and only primary tumors were used in the analysis. Study groups were divided based on *PTEN* status, HomDel (two copies with loss/mutation), HemDel (one copy loss or mutation), and Intact *PTEN* (both copies present without mutation). Differential expression (DE) analysis was carried out using DESeq2 (v 1.32.0) [30,31]. For enrichment analysis of DE genes, we used the clusterProfile package (v 3.18.1) [32,33]. We used a P-adjusted value < 0.05 as the cutoff for the enrichment results. All analyses were conducted in RStudio software (R Foundation for Statistical Computing, R v4.1.2) and all results were plotted by ggplot2 [34].

***In silico* analysis of immune abundance in tumor types**

To estimate the immune cell landscape in each tumor, we used the CIBERSORT deconvolution method (https://cibersort.stanford.edu/) that is an established tool to determine the abundance of immune cells using whole transcriptome data [35]. We separately imputed normalized gene expression data of brain, prostate, head and neck, stomach, cervical and colorectal tumors from the TCGA cohort.

RESULTS

PTEN alterations were present in 3413 (35.01%) 31 tumors comprising a total of 9,748 cases we analyzed from the TCGA PanCancer cohort (Figure 1, Supplementary Table 1). Copy number deletions were observed in 2685 (27.54%) tumors with 2292

(23.51%) hemizygous deletions affecting one copy and 393 (4.03%) having homozygous loss of both copies. Copy number gains as a duplication of the *PTEN* gene were evident in 728 (7.47%) tumors.

When stratified by tumor type, *PTEN* copy number alterations were more frequent in brain [combined grade IV gliomas (GBM) and low-grade gliomas (LGG)], kidney (KICH), uterine carcinosarcoma (UCS), lung squamous cell carcionoma (LUSC), ovarian serous cystadenocarcinoma (OV), sarcoma (SARC) and testicular germ cell tumors (TGCT) (Figure 1, Supplementary Table 1). *PTEN* copy number hemizygous deletions (HemDel) were more frequent in brain (35.34%), kidney (72.31%) and sarcoma (47.81%). While, *PTEN* copy number homozygous deletions (HomDel) were more frequent in prostate cancer (PRAD), lung squamous cell carcinoma (LUSC) and brain, respectively 17.42%, 9.92% and 3.31%. When we analyzed the copy number gain as a duplication of the *PTEN* gene (Dupl) was more frequent in uterine carcinosarcoma (UCS), adrenocortical carcinoma (ACC), uterine corpus endometrial carcinoma (UCEC) and ovarian serous cystadenocarcionoma (OV), respectively 32.14%, 13.92%, 20.85% and 19.66%.

To investigate whether *PTEN* deletions were associated with decreased *PTEN* expression, we compared RNAseq expression data between tumors with *PTEN* intact and *PTEN* deletions per cancer type. We found significantly decreased *PTEN* RNA expression in tumors harboring *PTEN* HomDel, such as in brain, cervix, colorectal, head and neck, prostate, sarcoma, and stomach (Figure 2a). We also investigated relative gene expression levels based on PTEN copy number for the entire cohort (Figure 2b). We observed that tumors with *PTEN* HemDel had significantly lower expression of *PTEN* compared with *PTEN* intact tumors. The HemDel, showing the expected intermediate expression levels compared to the marked reduced expression

levels observed for *PTEN* HomDel in all tumor types. *PTEN* gains classified as Dupl were associated with increased expression levels. These data are in good agreement with correlations observed between *PTEN* gene copy number and RNA expression levels using TCGA transcriptomic data that were reported by others [36].

PanCancer analysis of overall survival stratified by *PTEN* deletion status showed that tumors harboring *PTEN* HemDel had worse outcome compared with tumors with HomDel and PTEN intact ($P<0.0001$; Figure 3a). When stratified by tumor type, we also observed in brain tumors that both *PTEN* HomDel and HemDel were linked to earlier death events ($P<0.0001$; Figure 3b) and in cervical tumors we infer a lower survival probability for *PTEN* HemDel compared to HomDel and intact (Figure 3c). However, in colorectal tumors, both *PTEN* HemDel and *PTEN* intact showed the worse outcome compared with tumors with *PTEN* HomDel (Figure 3d). The same behavior is seen in prostate cancer and head and neck squamous cell carcinoma (Supplementary Figure 1a, 1b). Stomach tumors and sarcoma with *PTEN* HomDel presented earlier death events (Supplementary Figure 1c and 1d).

To understand the impact of *PTEN* loss on genomic features, we analyzed the total number of mutations, percent genome altered by losses and gains, intratumor heterogeneity, aneuploidy, and homologous repair defects (Figure 4 a-d). Our combined analysis of the TCGA cohort revealed that cancers harboring *PTEN* HemDel had the highest levels of nonsilent mutations, intratumor heterogeneity, and percent genome altered. Moreover, both *PTEN* HomDel and HemDel presented higher levels of homologous repair defect when compared with *PTEN* intact, but no difference was found between the two deletion types. In contrast, aneuploidy levels were significantly elevated in HemDel compared to HomDel and both deletion types showed significant increased aneuploidy compared to intact tumors (Supplementary Figure 2).

When stratified by tumor type, brain tumors harboring *PTEN* deletions had increased genomic alterations in comparison to *PTEN* intact (Supplementary Figure 3). In addition, brain tumors with *PTEN* HomDel had highest percent genome altered than hemizygous and intact tumors. Prostate tumors with *PTEN* HemDel, on the other hand, were associated with more genomic changes, as measured by percent genome altered, intratumor heterogeneity, nonsilent mutations, and homologous repair defects (Supplementary Figure 3). We also found that 65% (13/20) investigated tumor types presented higher percent genome altered when harboring *PTEN* HemDel. This finding led us to hypothesize if *PTEN* HemDel may be associated with an altered transcriptome which could be potentially driving more genomic alterations.

Thus, we then investigated the transcriptome of tumors that had more *PTEN* deletions and presented more diversity in genomic changes. Differential gene expression analyses showed that prostate tumors with *PTEN* HemDel presented 2076 upregulated and 2966 downregulated genes (Supplementary Table 2). Prostate tumors with HemDel of *PTEN* presented several enriched pathways compared with *PTEN* intact, including microtubule-based movement and chromosome segregation (Supplementary Figure 4). *PTEN* HemDel was associated with distinct enrichment of immune pathways across cancer types. Also, prostate tumors with *PTEN* HomDel showed a high number of DEGs, which were linked to cell cycle, DNA repair, and vascular process pathways (Supplementary Figure 5). Interestingly, this tumor type showed that the genes closely flanking *PTEN* such as *ATAD1, RNLS* and *KLLN* are concurrently down-regulated with the *PTEN* gene (see vertical bar in Supplementary Figure 5).

Brain tumors presented the most distinct pathway enrichment results, including the upregulation of several immune pathways when *PTEN* was deleted. In these tumors,

we found 7841 up- and 6623 downregulated genes when compared tumors with *PTEN* HemDel vs. *PTEN* intact (Supplementary Table 2, Supplementary Figure 6). GO enriched analysis showed that several immune-related pathways were upregulated for *PTEN* HemDel tumors, such as granulocyte migration and chemotaxis, neutrophil migration, acute inflammatory response, humoral immune homeostasis, and many others (Supplementary Figure 6). Similarly, when we compared the transcriptome of tumors with *PTEN* HomDel vs. those with PTEN intact, we observed 6115 up- and 5323 downregulated genes (Supplementary Table 2, Supplementary Figure 7). We also observed that several immune-related pathways were significantly upregulated in brain tumors harboring *PTEN* HomDel, namely myeloid leucocyte migration, humoral immune response, leucocyte chemotasis, acute inflammatory response (Supplementary Figure 7). In summary, the majority of investigated tumors had immune-related pathways up- or downregulated when *PTEN* was lost. The RNA-sequencing expression level of immunomodulatory genes like CD274 (PD-L1, Programmed Cell Death), CTLA4 (Cytotoxic T-Lymphocyte Associated Protein 4), IDO1 (Indoleamine 2,3-Dioxygenase 1), and LAG3 (Lymphocyte Activating 3) are altered in breast, glioblastoma, head and neck, liver, ovarian, prostate, sarcoma, stomach, and uterine tumors (Supplementary Figure 8). These findings led us to hypothesise whether *PTEN* genomic deletions may be associated with an altered tumor microenvironment, as determined from higher or lower abundance of immune cells surrounding cancerous lesions.

Stomach tumors harboring *PTEN* HemDel showing downregulated immune pathways, such as adaptive immune response, regulation of lymphocyte activation, T cell activation, positive regulation of immune response, leukocyte mediated immunity, lymphocyte proliferation, and several other pathways (Supplementary Figure 9).

Stomach tumors with *PTEN* HemDel also had a downregulation of Indoleamine 2,3-Dioxygenase 1 (*IDO1*) gene (Supplementary Figure 8). Conversely, these results were different from those found for stomach tumors harboring *PTEN* HomDel (Supplementary Figure 10). For head and neck tumors, we also observed that tumors with *PTEN* HemDel had downregulated immune-related pathways, including adaptive immune response, activation of T-cell receptor, regulation of lymphocyte-mediated immunity, regulation of leukocyte mediated immunith, and regulation of immune effector process (Supplementary Figure 11). However, these results were not observed for the comparison between *PTEN* HomDel and *PTEN* intact (Supplementary Figure 12). Lastly, for colon tumors, we found that tumors with *PTEN* HemDel had downregulated immune-related pathways, including response to interferon-gamma, lymphocyte mediated immunity, adaptive immune response, and natural killer cell mediated immunity (Supplementary Figure 13). However, these results were not observed for the comparison between *PTEN* HomDel and *PTEN* intact (Supplementary Figure 14).

The results from the tumor microenvironment comparison of *PTEN* HomDel, HemDel and intact tumors for all 22 immune cells from brain, prostate, head and neck and stomach tumors were investigated. *PTEN* HemDel in brain tumors was linked to higher T CD4 memory cells and M2 macrophages abundance and lower M1 macrophages, monocytes, and T CD8 cells (Supplementary Figure 15 a). Similar results were seen in head and neck tumors, where *PTEN* HemDel showed higher M0 and M2 macrophages and mast cells, and lower CD4+ T-cell, CD8+ T-cell, T-regulatory cells and NK cells (Supplementary Figure 16). While in prostate tumors with *PTEN* HemDel we observed an increased in M1 macrophages and decreased M0 macrophages and monocytes abundance (Supplementary Figure 15 b), stomach tumors with *PTEN*

HemDel had an increased plasma and M0 macrophages density and decreased density of CD8+ T-cells (Supplementary Figure 15 c). Cervical tumors with *PTEN* HemDel were linked to higher M0 macrophages and mast cells activated abundance (Supplementary Figure 15 d). Similar results were seen in colorectal tumors, where *PTEN* HemDel showed higher M0 macrophages density and lower CD8+ T-cell abundance (Supplementary Figure 15 e).

DISCUSSION

Presence of the PTEN protein is essential for controlling the tumor promoting activities of the PI3K/AKT pathway [1]. Deregulation of this signaling axis confers a strong selective advantage to tumors, so that loss of *PTEN* control by inactivating mutation or deletion is one of the most common somatic events in human cancer [4]. PTEN mutation is significantly related to advanced disease, chemotherapy resistance, and poor survival in patients with head and neck cancers, breast, melanoma, colorectal, esophageal, and prostate [17,37–42] so that its role as a predictive and prognostic cancer biomarker is increasingly gaining prominence [43].

Various murine models have shown that the tumor promoting abilities of loss of the *Pten* gene are strongly dose-dependent [44]. In some models the *Pten* gene loss has been found to exhibit haploinsufficiency with reduced levels of the normal Pten protein resulting in a diversity of tumors in mice [1]. Thus, in contrast to the classical definition of a tumor suppressor gene that requires complete loss of both copies of the gene [45], it appears that reduced amounts of PTEN protein caused by either monoallelic loss or by one inactivating mutation is sufficient to cause cancer (reviewed in [17]).

A recent review across all solid tumors showed that hemizygous *PTEN* loss due to monoallelic deletion or point mutation occurred at a much higher frequency than

biallelic loss [13]. Our *PTEN* analysis of TCGA data also shows that most tumors have a much greater frequency of HemDel than HomDel and that hemizygous loss is less favorable than homozygous loss for some tumor types. These data agree with previous genetic and proteomic studies of PI3K/AKT/mTOR axis mutations using TCGA data that showed outcome associated with partial loss of *PTEN* was less favorable than outcome for complete loss of the gene [16]. Our analysis of *PTEN* RNA transcript levels across the TCGA cohort show good agreement with gene copy number, as reported recently by others [36], so that the HemDel losses we analyzed in this study would be expected to reduce RNA expression levels. Moreover, since one somatic *PTEN* deletion or point mutations leads to a reduction in RNA levels, then partial PTEN protein expression is expected in HemDel tumors.

PTEN deletions and protein loss are known to affect DNA damage responses and disrupt mitotic spindle architecture resulting in accumulation of mutations in other genes and increased chromosome instability in both murine models and human cancers [46]. As expected, our TCGA analysis showed both hemi- and homozygous losses increased genomic instability features in many tumors. However, HemDel tumors had significantly higher rates of non-silent mutations, intratumor heterogeneity, percentage genome altered and aneuploidy compared to HomDel tumors. This diversity of genetic alteration is likely to facilitate genomic evolution and increase cancer progression, treatment resistance and poor outcome [47]. Collectively, these data suggest that the elevated levels of genomic instability and somatic mutations in the tumors with hemizygous loss could provide a selective advantage and the less favorable outcome we observe across the TCGA cohort.

The most obvious effects on outcome for HemDel *PTEN* losses were for head and neck squamous cell carcinomas (HNSCC), and cervical carcinomas. For both tumor

types, hemizygous loss was associated with a less favorable overall survival. *PTEN* loss is associated with poor outcome in HNSCC [38]. HNSCC also has a high frequency of *TP53* somatic mutations [48]. We used bioportal to investigate the co-occurrence frequencies of *TP53* mutations with *PTEN* intact, HemDel and HomDel in HNSCC. Interestingly, *PTEN* HemDel was significantly ($P<0.001$) associated with *TP53* mutation and *PTEN* HomDel was under-represented in HNSCC with mutated *TP53* (data not shown). These data suggest that there may be preferential selection for one copy of a *PTEN* gene in HNSCC so that reduced levels of the functional PTEN protein allow tumor cells to bypass the *TP53*-induced cell senescence pathway [49]. These observations in HNSCC are in keeping with the *PTEN* literature that suggests that single-copy inactivation of *PTEN* may actually be selected for during the progression of some tumor types, since bi-allelic inactivation of *PTEN* has been shown to lead to senescence or cell death when *TP53* is mutated [3]. Recent functional studies of the relationship between *TP53* mutation and *PTEN* loss in HNSCC indicates that loss of regulation of both pathways could influence radio- and chemosensitivity [50]. These findings are also in agreement with recent studies showing that *PTEN* loss mediates resistance to cetuximab in HNSCC, indicating the need for more treatment response *PTEN* predictive biomarker studies in this tumor that also examined the role of HemDel events [51].

Mouse models of HNSCC draw attention to the role of *Pten* in evasion of cellular senescence and activation of cancer-related inflammation [52]. Our gene set enrichment analysis for HNSCC indicates that various pathways involved with immune activation are downregulated in *PTEN* HemDel tumors. Pathways indicated in our analysis were antigen presentation, interferon, interleukins, toll like, neutrophil, B cell and inflammasome signaling. More marked alterations to immune response in HemDel

HNSCC was also evident in our CIBERSORT analysis. There was decreased CD8+ve T-cells and alterations to TAMs consistent with the immune tumor microenvironment being less favorable in hemizygous HNSCC. These findings are consistent with the emerging recognition that *PTEN* loss could be a useful predictive immunobiomarker in HNSCC [53].

Biomarker analysis of colorectal cancer showed weak expression of the PTEN protein in primary tumors was associated with acquisition metastatic disease [41]. Our study found that *PTEN* HemDel colorectal tumors had downregulated immune-related pathways. Functional activities associated with immune response included regulation of granulocyte-macrophage colony-stimulating factor production, neutrophil migration, regulation of leukocyte mediated cytotoxicity. These findings are consistent with recent studies that showed that PTEN mutation was associated with microsatellite stability/instability and tumor mutational burden in colon cancer [54]. Both *in vitro* studies [55] and recent analyses of colon tumors [56] suggest that *PTEN* loss in colorectal carcinoma may activation of PI3K and upregulate *PD-L1* expression. These data are in keeping with other studies indicating that the PTEN/ PI3K axis may promote immune escape through regulating *PDL1/PD1* expression [2,57].

Brain tumors also presented distinct pathway enrichment findings, including the upregulation of several immune pathways for *PTEN* HemDel and HomDel losses. These data are consistent with a recent study showing *PTEN* loss in glioblastoma was associated with immunosuppressive expression signatures and failed response to anti-PD-1 immunotherapy [58].

Our TCGA analysis of prostate tumors with *PTEN* HemDel identified elevated levels of genomic instability and an increase in M1 macrophages but decreased abundances of M0 macrophages and monocytes. Pathway analysis showed enrichment

for response to type I-interferon, consistent with other recent findings showing that *PTEN* loss leads to an immunosuppressive microenvironment in PCa [59]. These conclusions also agree with our previous study that showed increased IDO1 and Tregs in the prostate cancer tumor microenvironment [60]. Interestingly, analysis of PCa showed that the genes flanking *PTEN* such as *ATAD1, RNLS* and *KLLN* are concurrently down-regulated when the *PTEN* gene is homozygously deleted. Similar observations were mode in both colon and head and neck tumors with homozygous deletions. These data suggest that large somatic deletions of chromosome 10 may often encompass closely linked genes whose expression changes could contribute to clinical phenotypes [61].

Unfortunately, most previous *PTEN* cancer biomarker studies have not systematically analyzed mutations or deletions using molecular genetic methods that can distinguish between HemDel and HomDel mutations. Similarly, loss of the protein using immunohistochemistry as an alternative way of determining PTEN status has also not been studied using uniform, reproducible methods that can detect subtle changes in protein levels [13,15,23,24]. The end result has been that majority of published *PTEN* cancer biomarker studies have depended on a variety of simple two-way classification assays (*PTEN* loss vs. intact) that ignore the distinction between hemi- and homozygous losses.

Our study also has some limitations that need to be addressed in future *PTEN* analyes of the highlighted tumors. Our work was based entirely on *in silico* analysis of copy number data derived TCGA and all the pathway and immune parameters were inferred from the associated transcriptome data. The analysis presented here cannot fully capture the impact of PTEN mutations, based on the limitations of the TCGA dataset, which lacks prognostic or treatment information. Also, our expression analyses associated with *PTEN* status were, like all *in silico* TCGA studies, obtained from the bulk tumors containing heterogeneous tumor cells intermingled with small subset of

stromal cells, and varying quantities of immune cells. Lastly, our analysis regarding *PTEN* status did not include *PTEN* inversions, fusions, promoter methylations, and large-scale structural variants, which may be a source of bias in our evaluation of the impact of HemDel and HomDel effects.

Collectively, our findings based on TCGA, together with the extensive murine *Pten* studies by others [6,7], suggest that loss of one copy of *PTEN* by mutation or deletion may be sufficient to promote tumorigenesis. However, for most human cancers there is limited information on whether hemizygous *PTEN* loss plays a prognostic role or is associated with differential treatment responses.

LIST OF ABBREVIATIONS

ACC - Adrenocortical carcinoma

AKT - Protein kinase B

B cell – B lymphocyte

BLCA - Bladder Urothelial Carcinoma

BRCA - Breast invasive carcinoma

CD4 - Cluster of differentiation 4

CD8 - Cluster of differentiation 8

CESC - Cervical squamous cell carcinoma and endocervical adenocarcinoma

CGH - Comparative genomic hybridization

CHOL – Cholangiocarcinoma

COAD - Colon adenocarcinoma

DE - Differential expression

DEG – Differential expression genes

DLBC - Lymphoid Neoplasm Diffuse Large B - cell Lymphoma

DNA - Deoxyribonucleic acid

ESCA - Esophageal carcinoma

FISH - Fluorescence in situ hybridization

GO - Gene Ontology

GSEA - Gene set enrichment

HemDel - Hemizygous deletion

HNSC - Head and Neck squamous cell carcinoma

HomDel - Homozygous deletion

IDO1 - Indoleamine 2,3-Dioxygenase 1

KIRC - Kidney renal clear cell carcinoma

KIRP - Kidney renal papillary cell carcinoma

LAML - Acute Myeloid Leukemia

LCML - Chronic Myelogenous Leukemia

LGG - Brain Lower Grade Glioma

LIHC - Liver hepatocellular carcinoma

LOH - Loss of heterozygosity

LUAD - Lung adenocarcinoma

M0 macrophage - Macrophage type 0

M1 macrophage - Macrophage type 1

M2 macrophage - Macrophage type 2

MESO - Mesothelioma

mTOR - Mammalian target of rapamycin

NK - Natural killer

OV - Ovarian serous cystadenocarcinoma

PAAD - Pancreatic adenocarcinoma

PCPG - Pheochromocytoma and Paraganglioma

PD-L1 - Programmed death-ligand 1

PI3K - Phosphatidylinositol-4,5-Bisphosphate 3-Kinase

PIP3 - Phosphatidylinositol-3,4,5-trisphosphate

PTEN - Phosphatase and tensin homolog

READ - Rectum adenocarcinoma

RNA - Ribonucleic acid

RNAseq - RNA sequencing

SARC - Sarcoma

SCNA - Somatic copy number alterations

SKCM - Skin Cutaneous Melanoma

SNP - Single nucleotide polymorphisms

SNV - Single nucleotide variant

STAD - Stomach adenocarcinoma

T cell - T lymphocyte

T reg - Regulatory T lymphocyte

TAM - Tumor associated macrophage

TCGA - The Cancer Genome Atlas

TGCT - Testicular Germ Cell Tumors

THCA - Thyroid carcinoma

THYM - Thymoma

UCEC - Uterine Corpus Endometrial Carcinoma

UVM - Uveal Melanoma

DECLARATIONS

Ethics approval and consent to participate: Research Ethics Committee of the Clinical Hospital of the Faculty of Medicine of Ribeirão Preto, number 3.088.034

Consent for publication: Not applicable

Availability of data and materials: The datasets used and/or analyzed during the current study are available from the corresponding author on reasonable request.

Competing interests: The authors declare that they have no competing interests

Funding: This research was funded by FAPESP, grant numbers 2019/22912-8 (JAS), 2021/12271-5 (WLD), 2020/12816-9 (LPC), and by CNPq grant PQ-1D to JAS.

Authors' contributions: All authors contributed equally to the development of this study. All authors read and approved the final manuscript.

Acknowledgements: Not applicable

REFERENCES

1. Chalhoub, N. & Baker, S. J. PTEN and the PI3-kinase pathway in cancer. *Annu. Rev. Pathol.* **4**, 127–150 (2009).
2. Vidotto, T. *et al.* Emerging role of PTEN loss in evasion of the immune response to tumours. *Br. J. Cancer* **122**, 1732–1743 (2020).
3. Lee, Y., Chen, M. & Pandolfi, P. P. The functions and regulation of the PTEN tumour suppressor: new modes and prospects. *Nat. Rev. Mol. Cell Biol.* **19**, 547–562 (2018).
4. The ICGC/TCGA Pan-Cancer Analysis of Whole Genomes Consortium. Pan-cancer analysis of whole genomes. *Nature* **578**, 82–93 (2020).
5. Bignell, G. R. *et al.* Signatures of mutation and selection in the cancer genome. *Nature* **463**, 893–898 (2010).
6. Wang, S. *et al.* Prostate-specific deletion of the murine Pten tumor suppressor

gene leads to metastatic prostate cancer. *Cancer Cell* **4**, 209–221 (2003).

7. Kwabi-Addo, B. *et al.* Haploinsufficiency of the Pten tumor suppressor gene promotes prostate cancer progression. *Proc. Natl. Acad. Sci. U. S. A.* **98**, 11563–11568 (2001).

8. Kwon, C. H. *et al.* Pten haploinsufficiency accelerates formation of high-grade astrocytomas. *Cancer Res.* **68**, 3286–3294 (2008).

9. Alimonti, A. *et al.* Subtle variations in Pten dose determine cancer susceptibility. *Nat. Genet.* **42**, 454–458 (2010).

10. Shen-Li, H., Koujak, S., Szablocs, M. & Parsons, R. Reduction of Pten dose leads to neoplastic development in multiple organs of PtenshRNA mice. *Cancer Biol. Ther.* **10**, 1194–1200 (2010).

11. Carracedo, A., Alimonti, A. & Pandolfi, P. P. PTEN level in tumor suppression: How much is too little? *Cancer Res.* **71**, 629–633 (2011).

12. Masson, G. R. & Williams, R. L. Structural mechanisms of PTEN regulation. *Cold Spring Harb. Perspect. Med.* **10**, (2020).

13. Álvarez-Garcia, V., Tawil, Y., Wise, H. M. & Leslie, N. R. Mechanisms of PTEN loss in cancer: It's all about diversity. *Semin. Cancer Biol.* **59**, 66–79 (2019).

14. Brennan, C. W. *et al.* The somatic genomic landscape of glioblastoma. *Cell* **155**, 462–77 (2013).

15. Pulido, R. *et al.* Precise immunodetection of PTEN protein in human neoplasia. *Cold Spring Harb. Perspect. Med.* **9**, 1–30 (2019).

16. Zhang, Y. *et al.* A Pan-Cancer Proteogenomic Atlas of PI3K/AKT/mTOR Pathway Alterations. *Cancer Cell* **31**, 820-832.e3 (2017).

17. Berger, M. F. *et al.* The genomic complexity of primary human prostate cancer.

Nature **470**, 214–220 (2011).

18. Vidotto, T., Tiezzi, D. G. & Squire, J. A. Distinct subtypes of genomic PTEN deletion size influence the landscape of aneuploidy and outcome in prostate cancer. *Mol. Cytogenet.* **11**, 1 (2018).

19. Fan, C., Zhao, C., Shugen Li, F. W. & Wang, J. Significance of PTEN mutation in cellular process, prognosis, and drug selection in clear cell renal cell carcinoma. *Front. Oncol.* **9**, 1–9 (2019).

20. Sun, J., Li, S., Wang, F., Fan, C. & Wang, J. Identification of key pathways and genes in pten mutation prostate cancer by bioinformatics analysis. *BMC Med. Genet.* **20**, 1–9 (2019).

21. Imada, E. L. *et al.* Transcriptional landscape of PTEN loss in primary prostate cancer. *BMC Cancer* **21**, 1–13 (2021).

22. Lin, Z. *et al.* PTEN loss correlates with T cell exclusion across human cancers. *BMC Cancer* **21**, 1–14 (2021).

23. Jamaspishvili, T. *et al.* Clinical implications of PTEN loss in prostate cancer. *Nat. Rev. Urol.* **15**, 222–234 (2018).

24. Hocking, C. *et al.* Can we accurately report PTEN status in advanced colorectal cancer? *BMC Cancer* **14**, 1–7 (2014).

25. Colaprico, A. *et al.* TCGAbiolinks□: an R/Bioconductor package for integrative analysis of TCGA data. *Nucleic Acids Res.* **44**, 1–11 (2016).

26. Mermel, C. H. *et al.* GISTIC2.0 facilitates sensitive and confident localization of the targets of focal somatic copy-number alteration in human cancers. *Genome Biol.* **12**, 1–14 (2011).

27. Zack, T. I. *et al.* Pan-cancer patterns of somatic copy number alteration. *Nat. Genet.* **45**, 1134–1140 (2013).

28. Collado-Torres, L. *et al*. Reproducible RNA-seq analysis using recount2. *Nat. Biotechnol.* **35**, 319–321 (2017).

29. Imada, E. L. *et al.* Recounting the FANTOM CAGE-Associated Transcriptome. *Genome Res*. **30**, 1073–1081 (2020).

30. Love, M. I., Huber, W. & Anders, S. Moderated estimation of fold change and dispersion for RNA-seq data with DESeq2. *Genome Biol.* **15**, 1–21 (2014).

31. Zhu, A., Ibrahim, J. G. & Love, M. I. Heavy-Tailed prior distributions for sequence count data: Removing the noise and preserving large differences. *Bioinformatics* **35**, 2084–2092 (2019).

32. Liberzon, A. *et al.* The Molecular Signatures Database Hallmark Gene Set Collection. *Cell Syst.* **1**, 417–425 (2015).

33. Wu, T. *et al.* clusterProfiler 4.0: A universal enrichment tool for interpreting omics data. *Innov*. **2**, 100141 (2021).

34. Wickham, H. *ggplot2: Elegant Graphics for Data Analysis. Springer-Verlag New York. Media* vol. 35 (2016).

35. Newman, A. M. *et al.* Robust enumeration of cell subsets from tissue expression profiles. *Nat. Methods* 1–10 (2015) doi:10.1038/nmeth.3337.

36. Shao, X. *et al.* Copy number variation is highly correlated with differential gene expression: A pan-cancer study. *BMC Med. Genet.* **20**, 1–14 (2019).

37. da Costa, A. A. B. A. *et al.* Low PTEN expression is associated with worse overall survival in head and neck squamous cell carcinoma patients treated with chemotherapy and cetuximab. *Int. J. Clin. Oncol.* **20**, 282–289 (2015).

38. Nagata, Y. *et al*. PTEN activation contributes to tumor inhibition by trastuzumab, and loss of PTEN predicts trastuzumab resistance in patients. *Cancer Cell* **6**, 117–127 (2004).

39. Bucheit, A. D. *et al.* Complete loss of PTEN protein expression correlates with shorter time to brain metastasis and survival in stage IIIB/C melanoma patients with BRAFV600 mutations. *Clin. Cancer Res.* **20**, 5527–5536 (2014).

40. Tachibana, M. *et al.* Expression and Prognostic Significance of PTEN Product Protein in Patients with Esophageal Squamous Cell Carcinoma. *Cancer* **94**, 1955–1960 (2002).

41. Sawai, H. *et al.* Loss of PTEN expression is associated with colorectal cancer liver metastasis and poor patient survival. *BMC Gastroenterol.* **8**, 1–7 (2008).

42. Sircar, K. *et al.* PTEN genomic deletion is associated with p-Akt and AR signalling in poorer outcome, hormone refractory prostate cancer. *J. Pathol.* **218**, 505–513 (2009).

43. Bazzichetto, C. *et al.* Pten as a prognostic/predictive biomarker in cancer: An unfulfilled promise? *Cancers (Basel).* **11**, 1–22 (2019).

44. Carnero, A. & Paramio, J. M. The PTEN/PI3K/AKT Pathway in vivo, cancer mouse models. *Front. Oncol.* **4**, 1–10 (2014).

45. Wang, L. H., Wu, C. F., Rajasekaran, N. & Shin, Y. K. Loss of tumor suppressor gene function in human cancer: An overview. *Cell. Physiol. Biochem.* **51**, 2647–2693 (2018).

46. Hou, S. Q., Ouyang, M., Brandmaier, A., Hao, H. & Shen, W. H. PTEN in the maintenance of genome integrity: From DNA replication to chromosome segregation. *BioEssays* **39**, 1–9 (2017).

47. Salk, J. J., Fox, E. J. & Loeb, L. A. Mutational Heterogeneity in Human Cancers: Origin and Consequences. *Annu. Rev. Pathol. Mech. Dis.* **5**, 51–75 (2010).

48. Lawrence, M. S. *et al.* Comprehensive genomic characterization of head and neck squamous cell carcinomas. *Nature* **517**, 576–582 (2015).

49. Chen, Z. *et al.* Crucial role of p53-dependent cellular senescence in suppression of Pten-deficient tumorigenesis. *Nature* **436**, 725–730 (2005).

50. Vahabi, M. *et al.* MiR-96-5p targets PTEN expression affecting radio-chemosensitivity of HNSCC cells. *J. Exp. Clin. Cancer Res.* **38**, 1–16 (2019).

51. Izumi, H. *et al.* Pathway-specific genome editing of PI3K/mTOR tumor suppressor genes reveals that PTEN loss contributes to cetuximab resistance in head and neck cancer. *Mol. Cancer Ther*. **19**, 1562–1571 (2020).

52. Bian, Y. *et al.* Loss of TGF-β signaling and PTEN promotes head and neck squamous cell carcinoma through cellular senescence evasion and cancer-related inflammation. *Oncogene* **31**, 3322–3332 (2012).

53. dos Santos, L. V., Abrahão, C. M. & William, W. N. Overcoming Resistance to Immune Checkpoint Inhibitors in Head and Neck Squamous Cell Carcinomas. *Front. Oncol.* **11**, 1–16 (2021).

54. Serebriiskii, I. G. *et al.* Comprehensive characterization of PTEN mutational profile in a series of 34,129 colorectal cancers. *Nat. Commun.* **13**, (2022).

55. Song, M. *et al.* PTEN Loss Increases PD-L1 Protein Expression and Affects the Correlation between PD-L1 Expression and Clinical Parameters in Colorectal Cancer. *PLoS One* **8**, (2013).

56. Ugai, T. *et al.* Association of PIK3CA mutation and PTEN loss with expression of CD274 (PD-L1) in colorectal carcinoma . *Oncoimmunology* **10**, 1956173 (2021).

57. Lastwika, K. J. *et al.* Control of PD-L1 expression by oncogenic activation of the AKT-mTOR pathway in non-small cell lung cancer. *Cancer Res*. **76**, 227–238 (2015).

58. Zhao, J. *et al.* Immune and genomic correlates of response to anti-PD-1

immunotherapy in glioblastoma. *Nat. Med.* **25**, 462–469 (2019).

59. Imada, E. L. *et al.* Transcriptional landscape of PTEN loss in primary prostate cancer. *bioRxiv* 1–42 (2020) doi:10.1101/2020.10.08.332049.

60. Vidotto, T. . *et al.* PTEN-deficient prostate cancer is associated with an immunosuppressive tumor microenvironment mediated by increased expression of IDO1 and infiltrating FoxP3+ T regulatory cells. *Prostate* **1**, 1–11 (2019).

61. Poluri, R. T. K. & Audet-Walsh, É. Genomic deletion at 10q23 in prostate cancer: More than PTEN loss? *Front. Oncol.* **8**, 1–7 (2018).

Figures

Figure 1. Percentage of *PTEN* copy number deletions and inactivation among 31 TCGA tumor types studied (n=9747). *PTEN* copy number analysis showed that glioblastoma multiforme (GBM) and kidney chromophobe (KICH) presented the highest levels of hemizygous deletions. Prostate cancer (PRAD) presented the most prominent *PTEN* homozygous deletion percentage, followed by lung squamous cell carcinoma (LUSC) and GBM.

Figure 2. a) Somatic copy number alterations (SCNA) between tumors with *PTEN* intact and *PTEN* deletions per cancer type (n=9747). **b)** Somatic copy number alterations (SCNA) between tumors with *PTEN* intact and *PTEN* deletions for the PanCancer cohort.

Figure 3. Kaplan-Meier curves illustrate overall survival for both *PTEN* intact and *PTEN* deletions groups (HemDel and HomDel). **a)** PanCancer cohort shows a lower survival probability for *PTEN* HemDel compared to HomDel and intact (P<0.0001). **b)** Brain tumors (GBM + LGG) display that both HomDel and HemDel were linked to earlier death events (P<0.0001). **c)** Cervical tumors show a lower survival probability for *PTEN* HemDel compared to HomDel and intact. **d)** Colorectal tumors show a lower survival probability for *PTEN* HemDel compared to HomDel.

Figure 4. *PTEN* deletions are associated with **a)** increased mutation levels, **b)** intra tumor heterogeneity (ITH), **c)** homologous repair defects (HRD), and **d)** percent genome alteration. Hemizygous deletions of *PTEN* are associated with increased levels of genomic alterations compared with homozygous deletions. Intact *PTEN* showed the lowest levels of genomic alterations.

Supplementary figures

Supplementary Figure 1. Kaplan-Meier curves illustrate overall survival for both *PTEN* intact and *PTEN* deletions groups (HemDel and HomDel). **a)** Prostate cancer. **b)** Head and neck cancer. **c)** Stomach tumors. **d)** Sarcoma.

Supplementary Figure 2. Association between aneuploidy levels and *PTEN* inactivation status. **a)** *PTEN* inactivation is significantly associated with increased levels of aneuploidy. **b)** Aneuploidy score stratified by tumor type. Prostate and brain tumors showed the lowest levels of aneuploidy across tumor types. Aneuploidy levels were determined based on the length of copy number alterations and normalized by tumor type. The scores range from 0, which indicates low levels of chromosome aberrations (copy number gains and losses). On the other hand, high levels of aneuploidy indicate that the genome of these tumors is highly altered, with larger chromosome gains and losses occurring.

Supplementary Figure 3. *PTEN* deletions are associated with genomic alterations in each tumor type. **a)** Nonsilent mutations. **b)** Intratumor heterogeneity. **c)** Homologous repair defects. **d)** Percent genome altered.

Supplementary Figure 4. *PTEN* HemDel PRAD showed distinct transcriptome activity. **a)** Transcriptome heatmap exhibiting clustering of top 50 DEGs. **b)** Enriched GO (BP) pathways of the upregulated genes. **c)** Enriched GO (BP) pathways of the downregulated genes. The color scale in the heatmap represents the Z-score of the normalized read counts for each gene, where the red scale color indicates upregulated and blue low expressed genes. Enrichment analyses were performed using *clusterProfiler* and *p*-adjusted value = 0.05 as the cutoff. Tables show the top 10 most significant Gene Ontology (BP) terms.

Supplementary Figure 5. *PTEN* HomDel PRAD showed distinct transcriptome activity. **a)** Transcriptome heatmap exhibiting clustering of top 50 DEGs. **b)** Enriched GO (BP) pathways of the upregulated genes. **c)** Enriched GO (BP) pathways of the downregulated genes. The color scale in the heatmap represents the Z-score of the normalized read counts for each gene, where the red scale color indicates upregulated and blue low expressed genes. Enrichment analyses were performed using *clusterProfiler* and *p*-adjusted value = 0.05 as the cutoff. Tables show the top 10 most significant Gene Ontology (BP) terms. Vertical bar indicates the closely linked passenger genes (*ATAD1*, *RNLS* and *KLLN*) that are concurrently down-regulated when *PTEN* is lost by a large deletion of chromosome 10.

Supplementary Figure 6. *PTEN* HemDel Brain (GBM + LGG) showed distinct transcriptome activity. **a)** Transcriptome heatmap exhibiting clustering of top 50 DEGs. **b)** Enriched GO (BP) pathways of the upregulated genes. **c)** Enriched GO (BP) pathways of the downregulated genes. The color scale in the heatmap represents the Z-score of the normalized read counts for each gene, where the red scale color indicates upregulated and blue low expressed genes. Enrichment analyses were performed using *clusterProfiler* and *p*-adjusted value = 0.05 as the cutoff. Tables show the top 10 most significant Gene Ontology (BP) terms.

Supplementary Figure 7. *PTEN* HomDel Brain (GBM + LGG) showed distinct transcriptome activity. **a)** Transcriptome heatmap exhibiting clustering of top 50 DEGs. **b)** Enriched GO (BP) pathways of the upregulated genes. The color scale in the heatmap represents the Z-score of the normalized read counts for each gene, where the red scale color indicates upregulated and blue low expressed genes. Enrichment analyses were performed using *clusterProfiler* and *p*-adjusted value = 0.05 as the cutoff. Tables show the top 10 most significant Gene Ontology (BP) terms.

Supplementary Figure 8. The RNA-sequencing expression level of immunomodulatory genes *CD274* (*PD-L1*), *CTLA4*, *IDO1*, and *LAG3* in BRCA, GBM, HNSC, LIHC, OV, PRAD, SARC, STAD, and UCS. *: *p*-value < 0.05; **: *p*-value < 0.01, by Mann-Whitney test. *CD274* (*PD-L1*), Programmed Cell Death 1 Ligand 1; *CTLA4*, Cytotoxic T-Lymphocyte Associated Protein 4; *IDO1*, Indoleamine 2,3-Dioxygenase 1; LAG3, Lymphocyte Activating 3.

Supplementary Figure 9. *PTEN* HemDel STAD showed distinct transcriptome activity. **a)** Transcriptome heatmap exhibiting clustering of top 50 DEGs. **b)** Enriched GO (BP) pathways of the upregulated genes. **c)** Enriched GO (BP) pathways of the downregulated genes. The color scale in the heatmap represents the Z-score of the normalized read counts for each gene, where the red scale color indicates upregulated and blue low expressed genes. Enrichment analyses were performed using *clusterProfiler* and *p*-adjusted value = 0.05 as the cutoff. Tables show the top 10 most significant Gene Ontology (BP) terms.

Supplementary Figure 10. *PTEN* HomDel STAD showed distinct transcriptome activity. **a)** Transcriptome heatmap exhibiting clustering of top 50 DEGs. **b)** Enriched GO (BP) pathways of the upregulated genes. The color scale in the heatmap represents the Z-score of the normalized read counts for each gene, where the red scale color indicates upregulated and blue low expressed genes. Enrichment analyses were performed using *clusterProfiler* and *p*-adjusted value = 0.05 as the cutoff. Tables show the top 10 most significant Gene Ontology (BP) terms.

Supplementary Figure 11. *PTEN* HemDel HNSC showed distinct transcriptome activity. **a)** Transcriptome heatmap exhibiting clustering of top 50 DEGs. **b)** Enriched GO (BP) pathways of the upregulated genes. **c)** Enriched GO (BP) pathways of the downregulated genes. The color scale in the heatmap represents the Z-score of the normalized read counts for each gene, where the red scale color indicates upregulated and blue low expressed genes. Enrichment analyses were performed using *clusterProfiler* and *p*-adjusted value = 0.05 as the cutoff. Tables show the top 10 most significant Gene Ontology (BP) terms.

Supplementary Figure 12. *PTEN* HomDel HNSC showed distinct transcriptome activity. **a)** Transcriptome heatmap exhibiting clustering of top 50 DEGs. **b)** Enriched GO (BP) pathways of the upregulated genes. **c)** Enriched GO (BP) pathways of the downregulated genes. The color scale in the heatmap represents the Z-score of the normalized read counts for each gene, where the red scale color indicates upregulated and blue low expressed genes. Enrichment analyses were performed using *clusterProfiler* and *p*-adjusted value = 0.05 as the cutoff. Tables show the top 10 most significant Gene Ontology (BP) terms. Vertical bar indicates the two closely linked passenger genes (*MINPP1 and KLLN*) that are concurrently down-regulated when PTEN is lost by a large deletion of chromosome 10.

Supplementary Figure 13. *PTEN* HemDel COAD showed distinct transcriptome activity. **a)** Transcriptome heatmap exhibiting clustering of top 50 DEGs. **b)** Enriched GO (BP) pathways of the downregulated genes. The color scale in the heatmap represents the Z-score of the normalized read counts for each gene, where the red scale color indicates upregulated and blue low expressed genes. Enrichment analyses were performed using *clusterProfiler* and *p*-adjusted value = 0.05 as the cutoff. Tables show the top 10 most significant Gene Ontology (BP) terms.

Supplementary Figure 14. *PTEN* HomDel COAD showed distinct transcriptome activity. **a)** Transcriptome heatmap exhibiting clustering of top 50 DEGs. Vertical bar indicates the closely linked passenger genes (*ALDH18A1, DNMBP, KLLN, WAPL, MINPP1, ATAD1)* that are concurrently down-regulated when PTEN is lost by a large deletion of chromosome 10.

Supplementary Figure 15. CIBERSORT□derived immune□cell abundance of 22 distinct cell subsets based on *PTEN* status and tumor type. Y□axis shows CIBERSORT relative scores. **a)** *PTEN* HemDel in brain tumors was linked to higher T CD4 memory cells and M2 macrophage abundance and lower M1 macrophages, monocytes, and T CD8 cells. **b)** Prostate tumors with *PTEN* HemDel showed increased M1 macrophages and decreased M0 macrophages and monocytes. **c)** Stomach tumors with *PTEN* HemDel showed increased plasma and M0 macrophages and decreased in T CD8 cells. d**)** Cervical tumors with *PTEN* HemDel were linked to higher M0 macrophages and

mast cells activated. **e)** Colorectal tumors with *PTEN* HemDel were linked to higher M0 macrophages and lower T CD8 cells. DC, dendritic cell; NK, natural-killer cell; PCa, prostate cancer; Treg, regulatory T cell; M0, M0 macrophage; M1, M1 macrophage; M2, M2 macrophage. *: *p*-value < 0.05; **: *p*-value < 0.01, by Mann-Whitney test.

Supplementary Figure 16. CIBERSORT-derived immune-cell abundance of 22 distinct cell subsets based on *PTEN* status and head and neck tumors. Y-axis shows CIBERSORT relative scores. *PTEN* HemDel in head and neck tumors was linked to higher M0 and M2 macrophages and mast cells, and lower T CD4, T CD8, T regs, and NK cells. DC, dendritic cell; NK, natural-killer cell; PCa, prostate cancer; Treg, regulatory T cell; M0, M0 macrophage; M1, M1 macrophage; M2, M2 macrophage. *: *p*-value < 0.05; **: *p*-value < 0.01, by Mann-Whitney test. n=10713

Supplementary tables

Supplementary Table 1. *PTEN* copy number status (CN). HemDel: *PTEN* hemizygous deletion. HomDel: *PTEN* homozygous deletion. *Dupl* Duplication or gain.

Supplementary Table 2. The number of differentially expressed genes (DEGs) by tumor and *PTEN* deletion status. FDR < 0.05. HemDel: *PTEN* hemizygous deletion. HomDel: *PTEN* homozygous deletion. Int: *PTEN* intact.

Figure 1

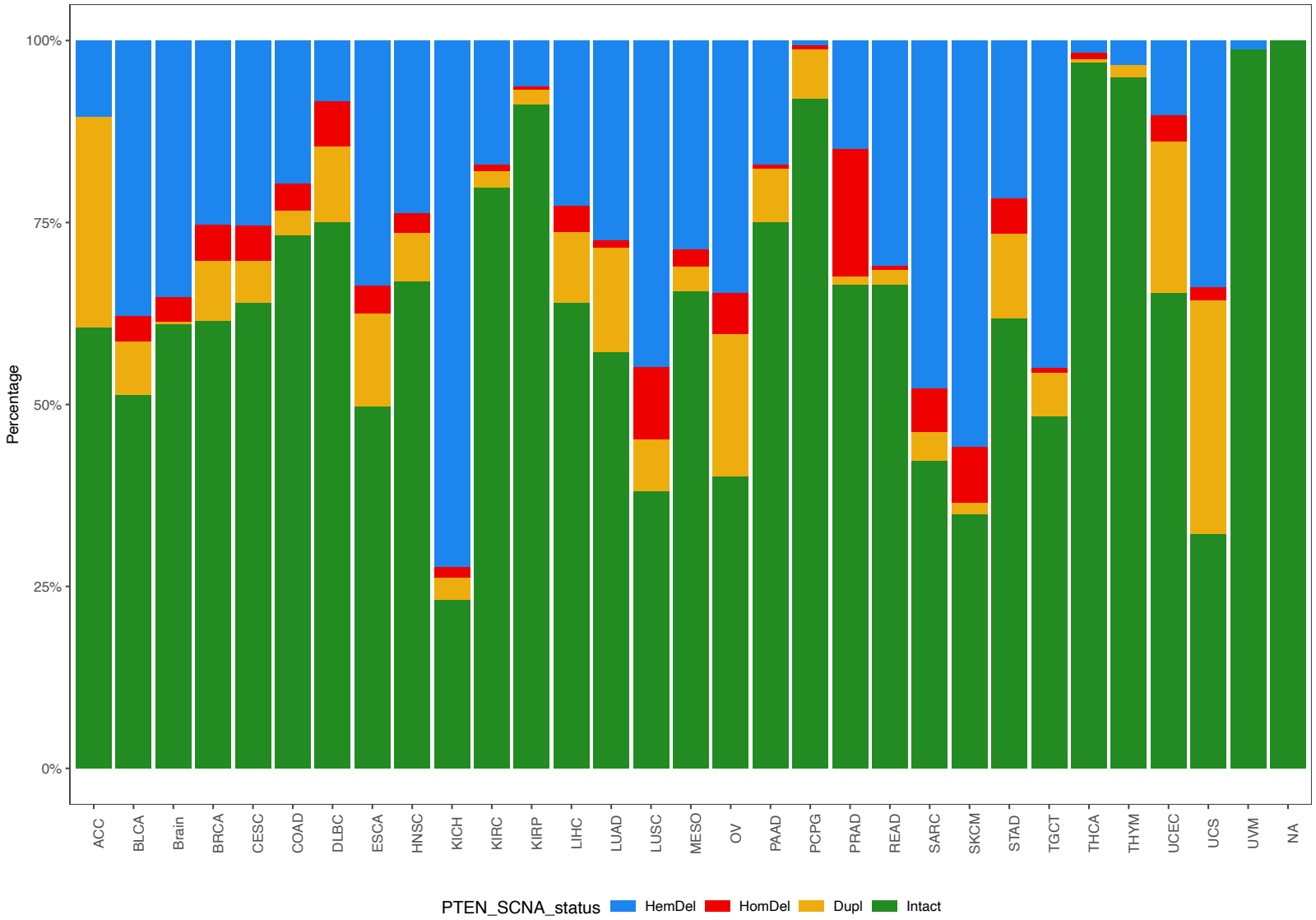
100%
75%
50%
25%
0%
Percentage
ACC
BLCA
Brain
BRCA
CESC
COAD
DLBC
ESCA
HNSC
KICH
KIRC
KIRP
LIHC
LUAD
LUSC
MESO
OV
PAAD
PCPG
PRAD
READ
SARC
SKCM
STAD
TGCT
THCA
THYM
UCEC
UCS
UVM
NA
PTEN_SCNA_status
HemDel
HomDel
Dupl
Intact

Figure 2

a

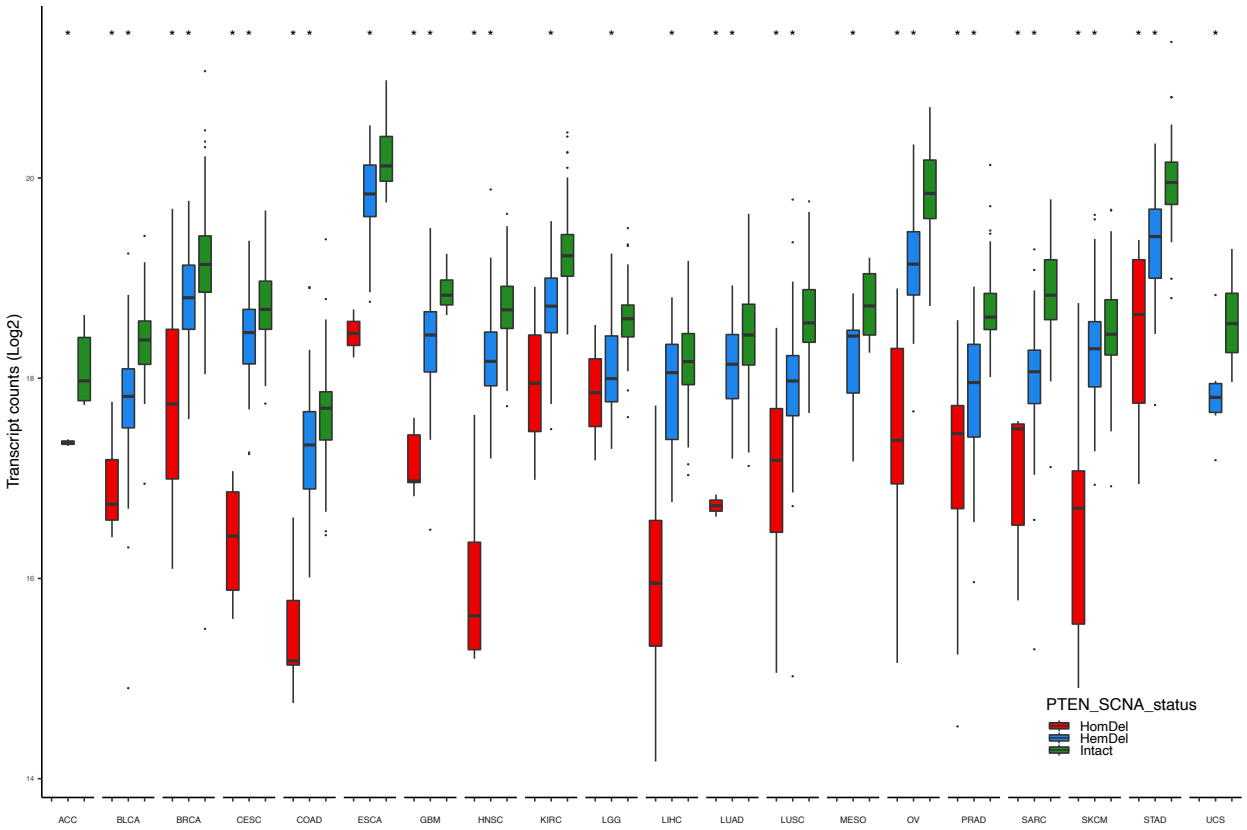
Transcript counts (Log2)
20
18
16
14
ACC
BLCA
BRCA
CESC
COAD
ESCA
GBM
HNSC
KIRC
LGG
LIHC
LUAD
LUSC
MESO
OV
PRAD
SARC
SKCM
STAD
UCS
PTEN_SCNA_status
HomDel
HemDel
Intact

b

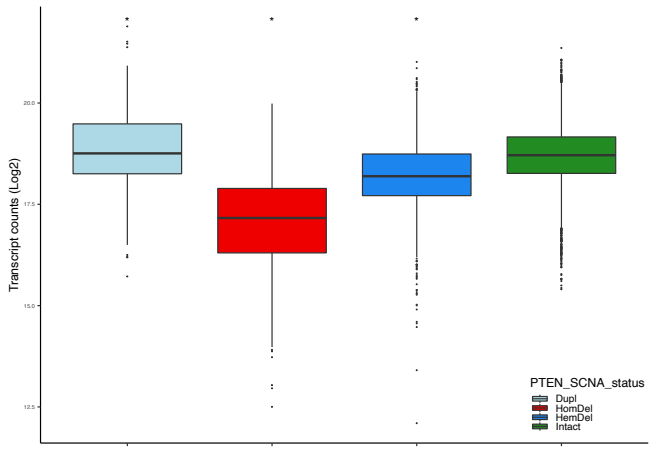
Transcript counts (Log2)
20.0
17.5
15.0
12.5
PTEN_SCNA_status
Dupl
HomDel
HemDel
Intact

Figure 3

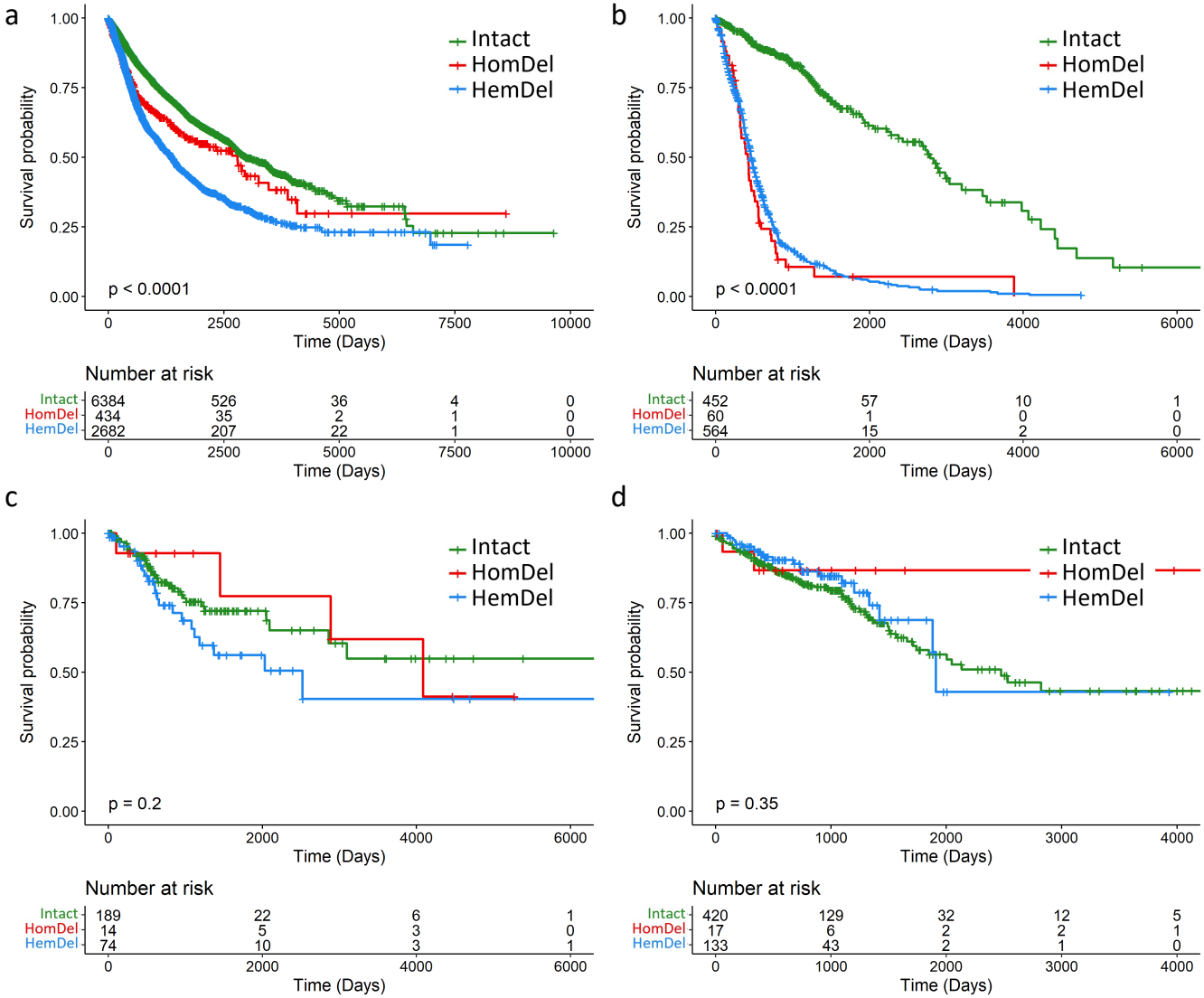
a
Survival probability
1.00
0.75
0.50
0.25
0.00
Intact
HomDel
HemDel
p < 0.0001
0
2500
5000
7500
10000
Time (Days)
Number at risk
Intact 6384 526 36 4 0
HomDel 434 35 2 1 0
HemDel 2682 207 22 1 0
b
p < 0.0001
0
2000
4000
6000
Number at risk
Intact 452 57 10 1
HomDel 60 1 0 0
HemDel 564 15 2 0
c
p = 0.2
Number at risk
Intact 189 22 6 1
HomDel 14 5 3 0
HemDel 74 10 3 1
d
p = 0.35
0
1000
2000
3000
4000
Number at risk
Intact 420 129 32 12 5
HomDel 17 6 2 2 1
HemDel 133 43 2 1 0

Figure 4

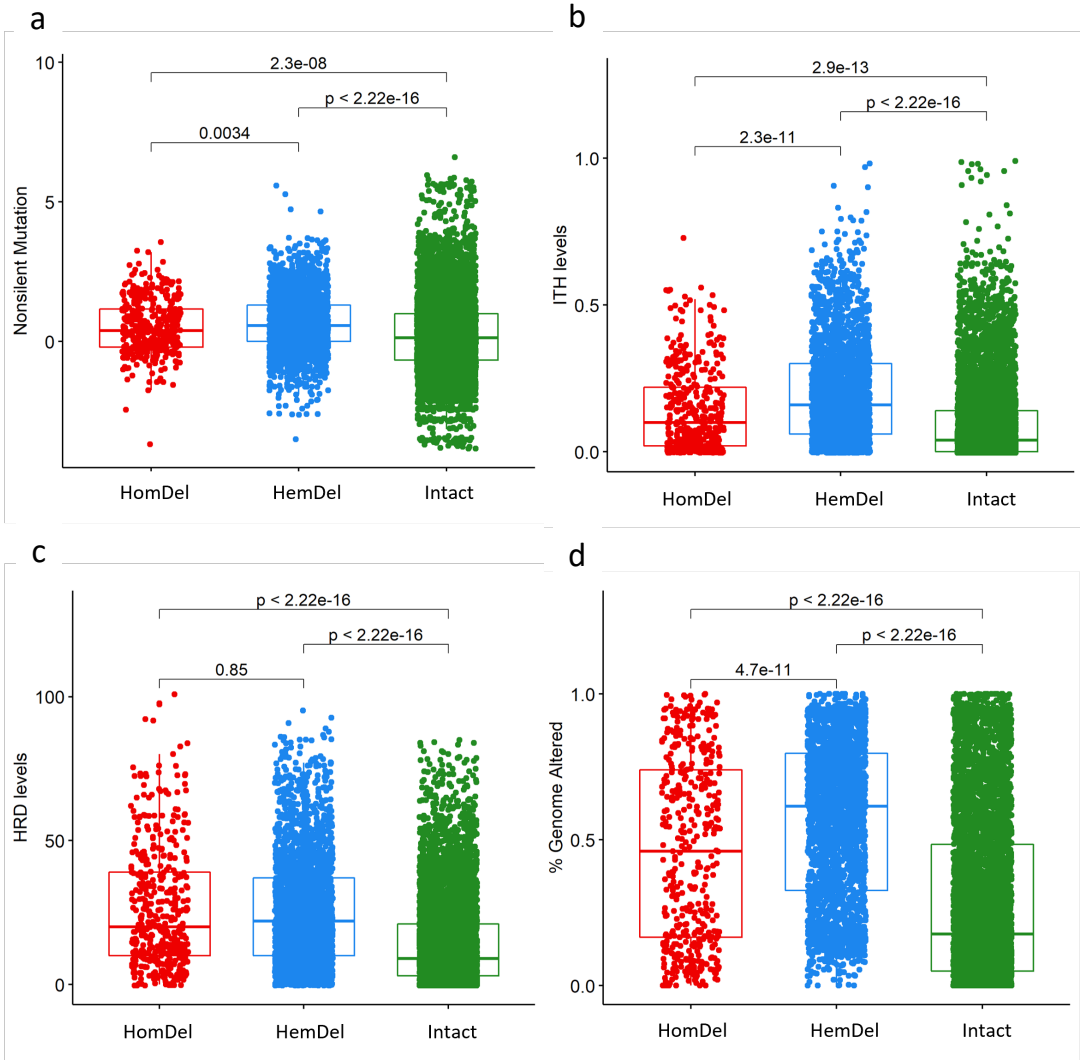
a
Nonsilent Mutation
10
5
0
2.3e-08
p < 2.22e-16
0.0034
HomDel
HemDel
Intact
b
ITH levels
1.0
0.5
0.0
2.9e-13
p < 2.22e-16
2.3e-11
HomDel
HemDel
Intact
c
HRD levels
100
50
0
p < 2.22e-16
p < 2.22e-16
0.85
HomDel
HemDel
Intact
d
% Genome Altered
1.0
0.5
0.0
p < 2.22e-16
p < 2.22e-16
4.7e-11
HomDel
HemDel
Intact

Supplementary figures and tables

Supplementary table 1

	PTEN CN Status								
TCGA Study	HemDe	%	HomDe	%	Dupl	%	Intact	%	Total
ACC	9	3,80	1	0,42	33	13,92	194	81,86	237
BLCA	153	37,87	14	3,47	30	7,43	207	51,24	404
BRCA	269	25,26	54	5,07	87	8,17	655	61,50	1065
CESC	74	25,43	14	4,81	17	5,84	186	63,92	291
CHOL	6	16,67	0	0,00	5	13,89	25	69,44	36
COAD	86	19,72	16	3,67	15	3,44	319	73,17	436
DLBC	4	8,33	3	6,25	5	10,42	36	75,00	48
ESCA	61	33,70	7	3,87	23	12,71	90	49,72	181
Brain	235	35,34	22	3,31	2	0,30	406	61,05	665
HNSC	117	23,78	13	2,64	33	6,71	329	66,87	492
KICH	47	72,31	1	1,54	2	3,08	15	23,08	65
KIRC	86	17,03	5	0,99	11	2,18	403	79,80	505
KIRP	18	6,36	1	0,35	6	2,12	258	91,17	283
LAML	1	0,83	2	1,67	2	1,67	115	95,83	120
LIHC	82	22,71	13	3,60	35	9,70	231	63,99	361
LUAD	140	27,50	5	0,98	73	14,34	291	57,17	509
LUSC	217	44,83	48	9,92	35	7,23	184	38,02	484
MESO	25	28,74	2	2,30	3	3,45	57	65,52	87
OV	143	34,71	23	5,58	81	19,66	165	40,05	412
PAAD	30	17,05	1	0,57	13	7,39	132	75,00	176
PCPG	1	0,62	1	0,62	11	6,83	148	91,93	161
PRAD	73	14,96	85	17,42	6	1,23	324	66,39	488
READ	48	30,97	1	0,65	3	1,94	103	66,45	155
SARC	120	47,81	15	5,98	10	3,98	106	42,23	251
STAD	90	21,74	20	4,83	48	11,59	256	61,84	414
TGCT	72	46,75	1	0,65	9	5,84	72	46,75	154
THCA	8	1,62	5	1,01	2	0,40	480	96,97	495
THYM	4	3,36	0	0,00	2	1,68	113	94,96	119
UCEC	53	10,23	19	3,67	108	20,85	338	65,25	518
UCS	19	33,93	1	1,79	18	32,14	18	32,14	56
UVM	1	1,25	0	0,00	0	0,00	79	98,75	80
	2292	23,51	393	4,03	728	7,47	6335	64,99	9748

Supplementary table 2

				DE Genes (HemDel vs Intact)		DE Genes (HomDel vs Intact)	
Tumor type	HemDel	HomDel	Int	Up	Down	Up	Down
Brain	235	22	406	7841	6623	6115	5323
Colorectal	86	16	319	1086	1536	23	175
Cervix	74	14	186	728	649	743	512
Head and Neck	117	13	329	1727	1842	444	1148
Prostate	73	85	324	2076	2966	3304	3835
Sarcoma	120	15	106	2032	3725	241	708
Stomach	90	20	256	3216	2814	683	1434
	795	185	1926	18706	20155	11553	13135

Supplementary figure 1

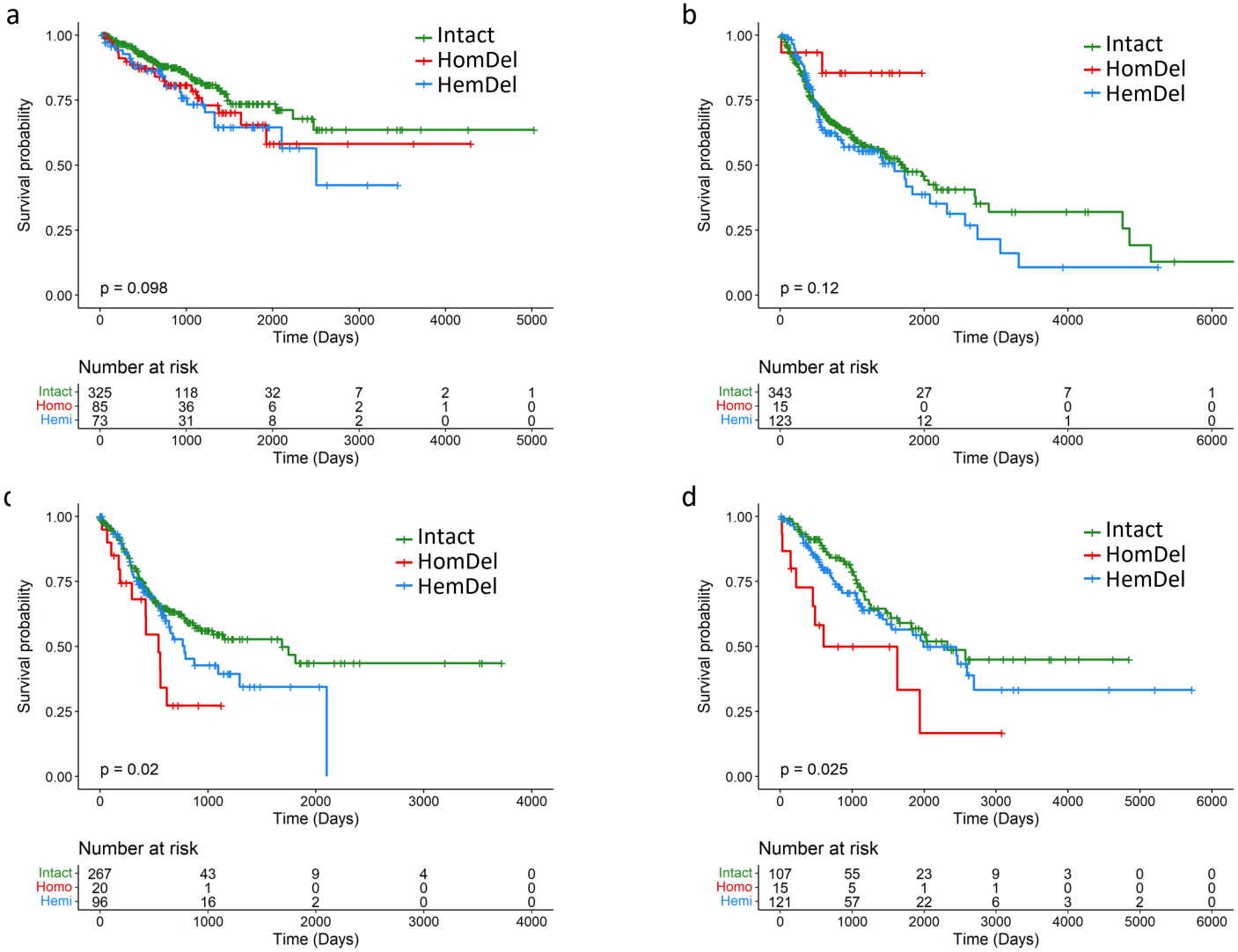

Supplementary figure 2

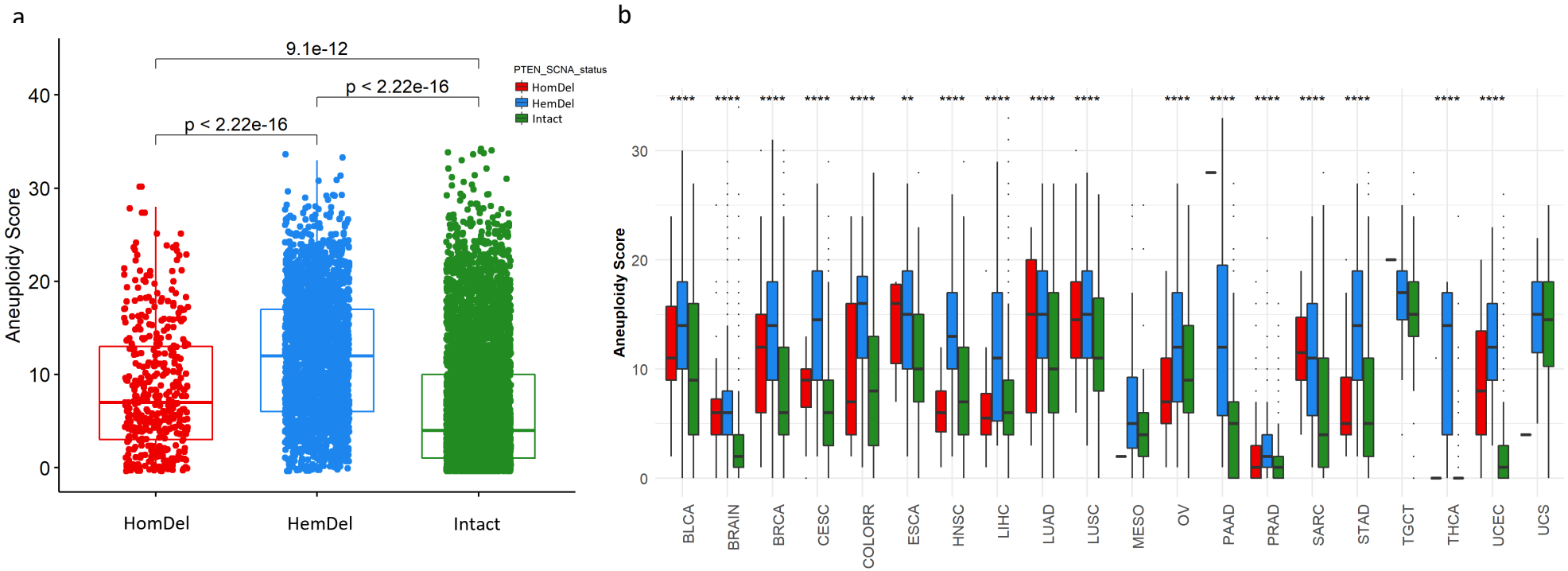

Supplementary figure 3

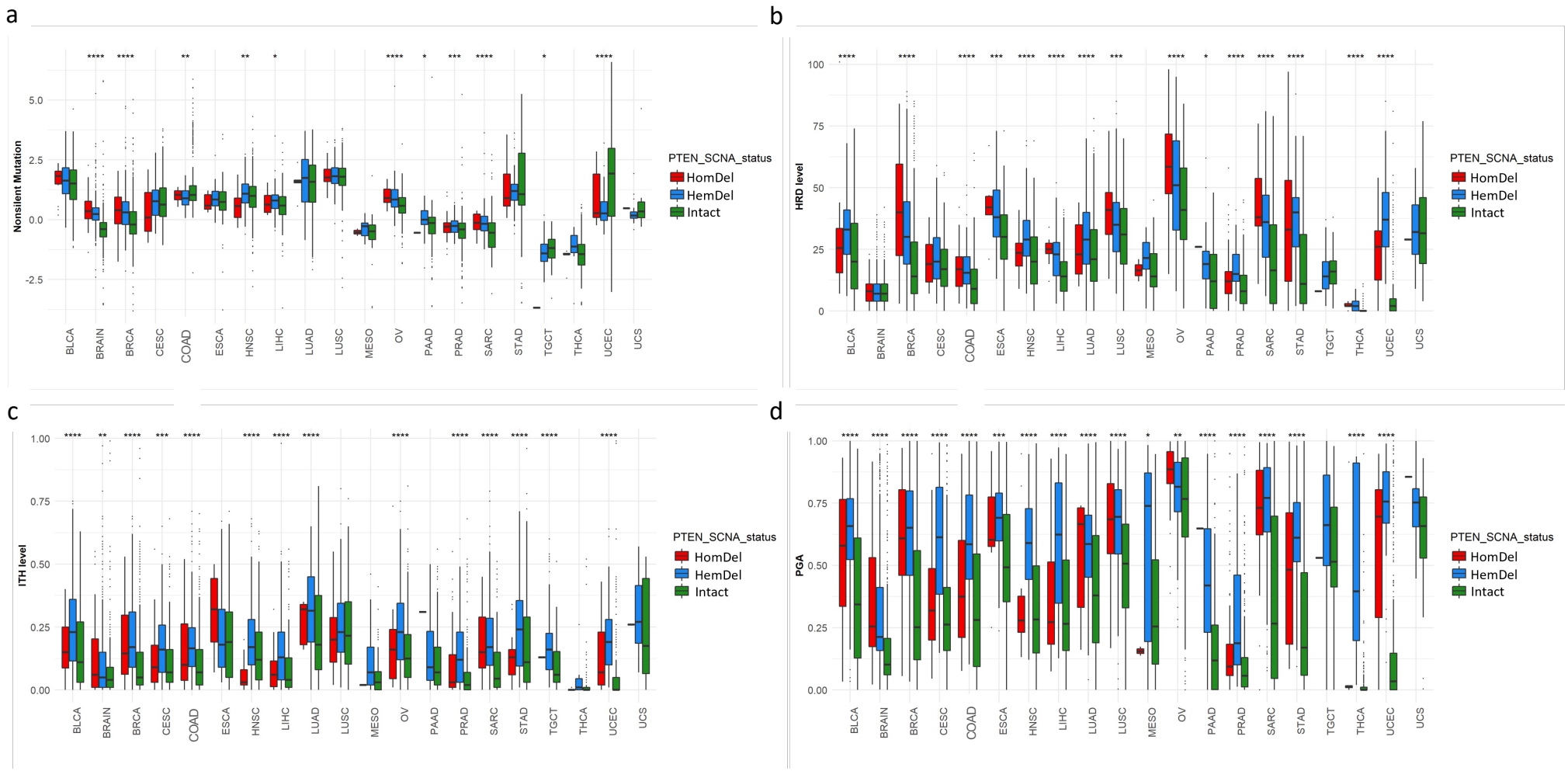

Supplementary figure 4

a

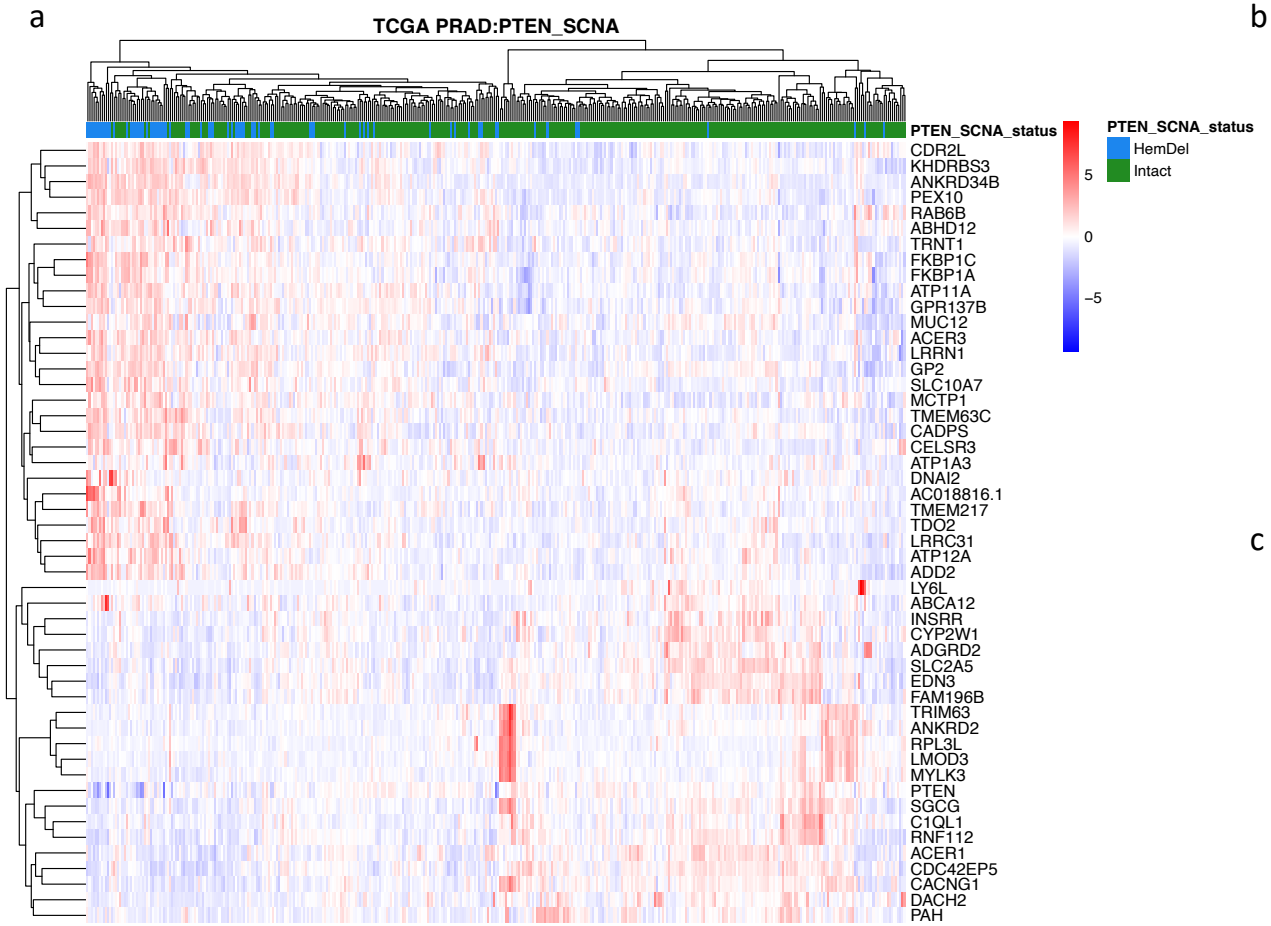

b

ID	Description	qvalue
GO:0007018	microtubule-based movement	3,41E+11
GO:0007059	chromosome segregation	3,41E+11
GO:0000070	mitotic sister chromatid segregation	3,41E+11
GO:0098813	nuclear chromosome segregation	0.0011
GO:1902850	microtubule cytoskeleton organization involved in mitosis	0.0015
GO:0034329	cell junction assembly	0.0018
GO:0050808	synapse organization	0.0028
GO:0032886	regulation of microtubule-based process	0.0038
GO:0000280	nuclear division	0.0065
GO:0007156	homophilic cell adhesion via plasma membrane adhesion molecules	0.0072

c

ID	Description	qvalue
GO:0002181	cytoplasmic translation	3,03E+07
GO:0006936	muscle contraction	1,28E+10
GO:0016054	organic acid catabolic process	1,86E+11
GO:0044282	small molecule catabolic process	8,90E+11
GO:0008015	blood circulation	0.0020
GO:0086005	ventricular cardiac muscle cell action potential	0.0070
GO:0010273	detoxification of copper ion	0.0154
GO:1990169	stress response to copper ion	0.0154
GO:0061687	detoxification of inorganic compound	0.0174
GO:0086009	membrane repolarization	0.0174

Supplementary figure 5

a

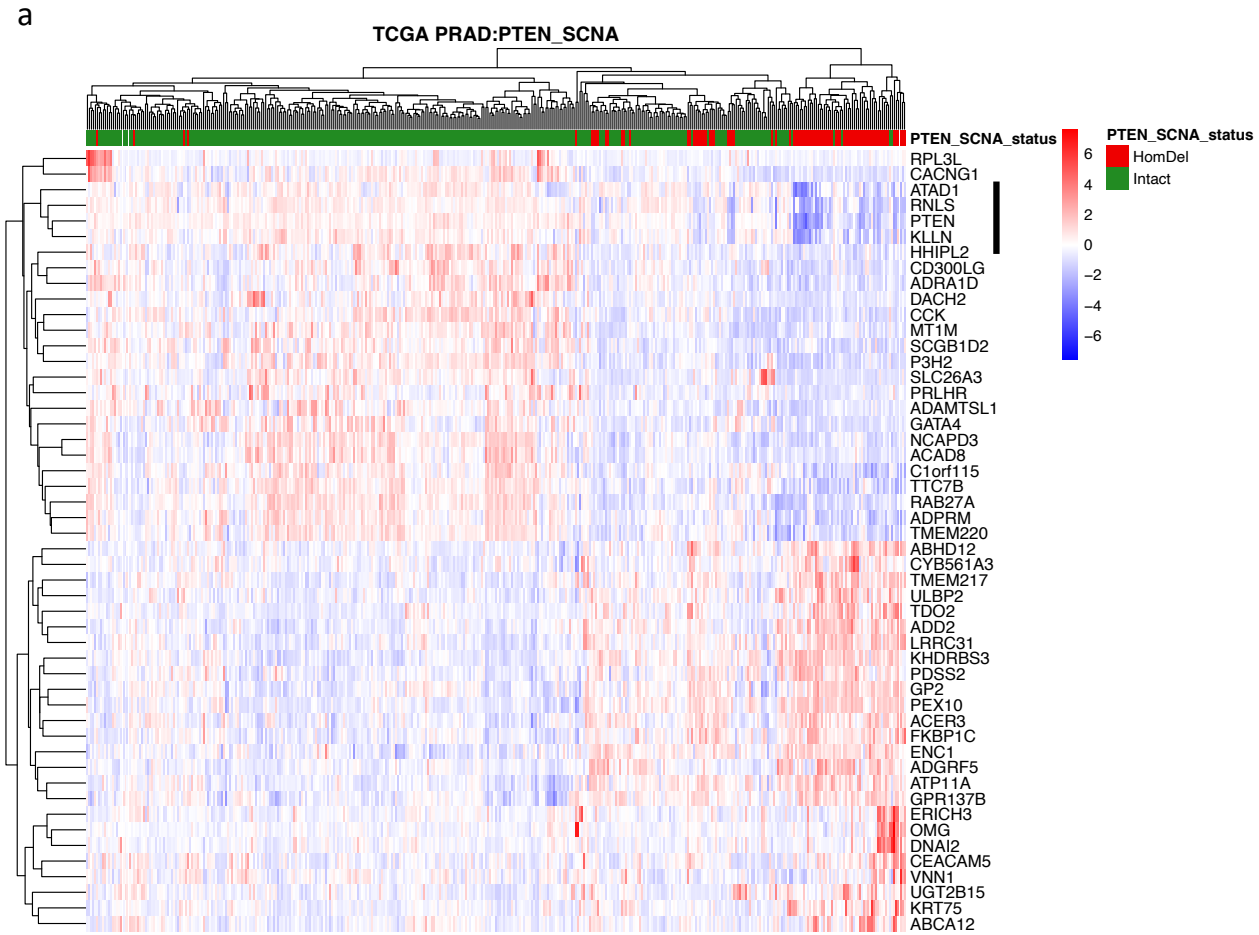

b

ID	Description	qvalue
GO:0044770	cell cycle phase transition	1,09E+12
GO:0007059	chromosome segregation	1,39E+12
GO:0007018	microtubule-based movement	2,92E+11
GO:1901987	regulation of cell cycle phase transition	4,63E+12
GO:0006281	DNA repair	6,03E+11
GO:0000819	sister chromatid segregation	0.0017
GO:0000070	mitotic sister chromatid segregation	0.0017
GO:0044782	cilium organization	0.0017
GO:0001578	microtubule bundle formation	0.0020
GO:0048285	organelle fission	0.0033

c

ID	Description	qvalue
GO:0008015	blood circulation	8,75E+09
GO:0006936	muscle contraction	1,16E+11
GO:0003018	vascular process in circulatory system	3,47E+11
GO:0034765	regulation of ion transmembrane transport	4,05E+11
GO:0099177	regulation of trans-synaptic signaling	0.0011
GO:0015844	monoamine transport	0.0022
GO:0008016	regulation of heart contraction	0.0038
GO:0016054	organic acid catabolic process	0.0041
GO:0072503	cellular divalent inorganic cation homeostasis	0.0041
GO:0007188	adenylate cyclase-modulating G protein-coupled receptor signaling pathway	0.0041

Supplementary figure 6

a

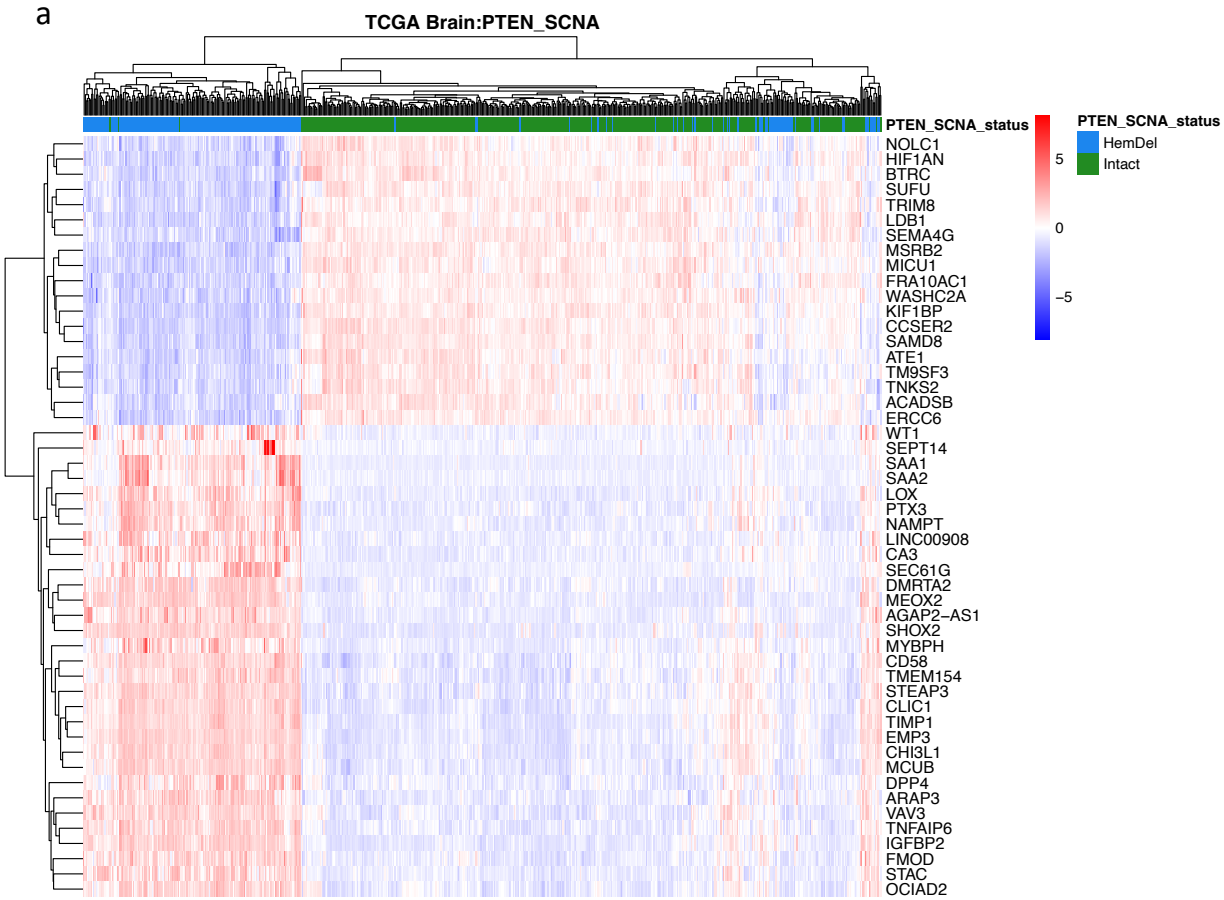

b

ID	Description	qvalue
GO:0002250	adaptive immune response	9,17E-10
GO:0042110	T cell activation	3,96E-06
GO:0030198	extracellular matrix organization	5,64E-05
GO:0002443	leukocyte mediated immunity	2,69E-01
GO:0002237	response to molecule of bacterial origin	4,85E-01
GO:0045785	positive regulation of cell adhesion	6,54E-02
GO:1903037	regulation of leukocyte cell-cell adhesion	7,12E-02
GO:0007159	leukocyte cell-cell adhesion	1,31E+00
GO:0050900	leukocyte migration	1,39E-01
GO:0050863	regulation of T cell activation	2,64E+00

c

ID	Description	qvalue
GO:0022613	ribonucleoprotein complex biogenesis	1,67E+08
GO:0008380	RNA splicing	1,67E+08
GO:0050804	modulation of chemical synaptic transmission	2,70E+10
GO:0099003	vesicle-mediated transport in synapse	6,22E+09
GO:0022618	ribonucleoprotein complex assembly	8,34E+09
GO:0071826	ribonucleoprotein complex subunit organization	1,97E+11
GO:0050808	synapse organization	5,09E+10
GO:0016197	endosomal transport	5,10E+11
GO:0043543	protein acylation	7,89E+10
GO:0001505	regulation of neurotransmitter levels	8,50E+11

Supplementary figure 7

a

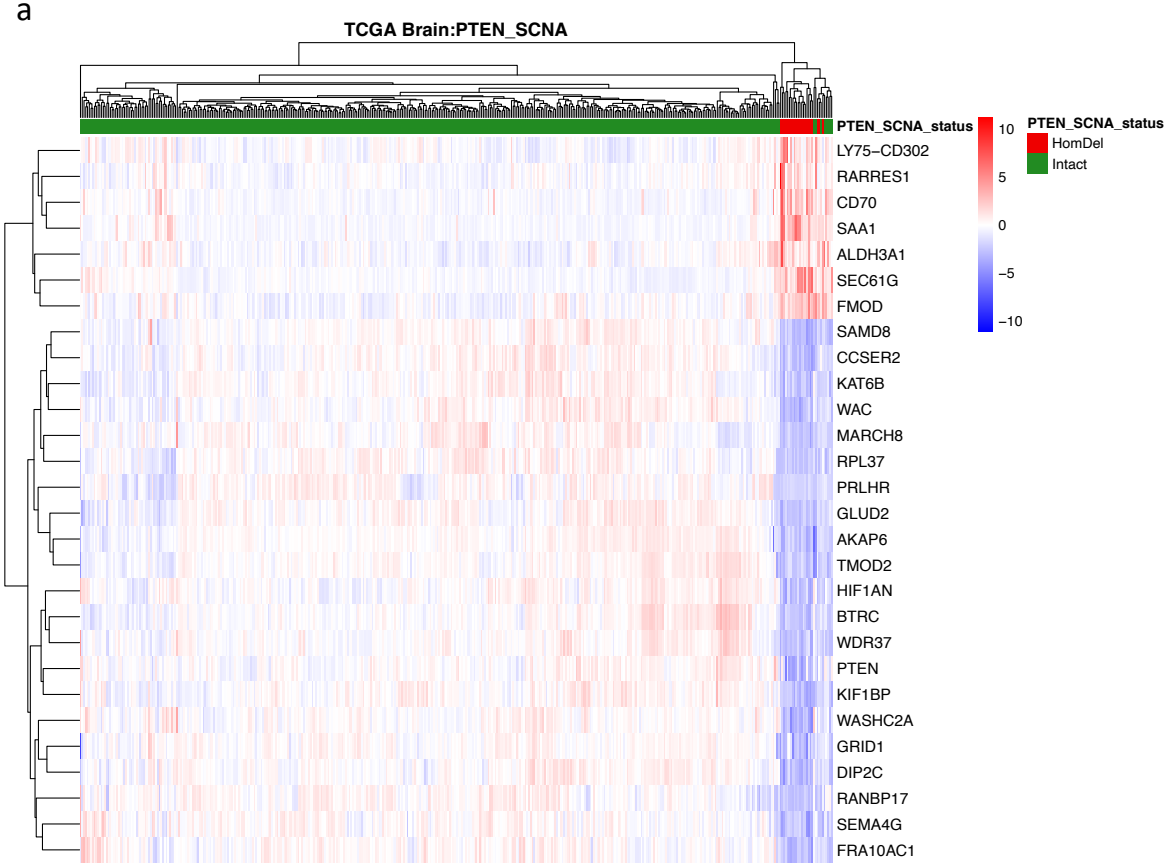

b

ID	Description	qvalue
GO:0002250	adaptive immune response	4,71E-13
GO:0042110	T cell activation	2,76E-09
GO:0050867	positive regulation of cell activation	3,49E-08
GO:0002443	leukocyte mediated immunity	7,82E-08
GO:1903037	regulation of leukocyte cell-cell adhesion	2,31E-06
GO:0050778	positive regulation of immune response	3,60E-05
GO:0007159	leukocyte cell-cell adhesion	7,56E-06
GO:0019221	cytokine-mediated signaling pathway	7,58E-06
GO:0050870	positive regulation of T cell activation	1,71E-02
GO:0001819	positive regulation of cytokine production	1,10E-01

c

ID	Description	qvalue
GO:0050804	modulation of chemical synaptic transmission	1,60E+01
GO:0099177	regulation of trans-synaptic signaling	1,60E+01
GO:0099504	synaptic vesicle cycle	2,43E+03
GO:0050808	synapse organization	9,90E+04
GO:0006397	mRNA processing	2,35E+08
GO:0016079	synaptic vesicle exocytosis	2,35E+08
GO:0060078	regulation of postsynaptic membrane potential	7,11E+07
GO:0099643	signal release from synapse	1,55E+09
GO:0016358	dendrite development	5,48E+08
GO:0001505	regulation of neurotransmitter levels	1,31E+09

Supplementary figure 8

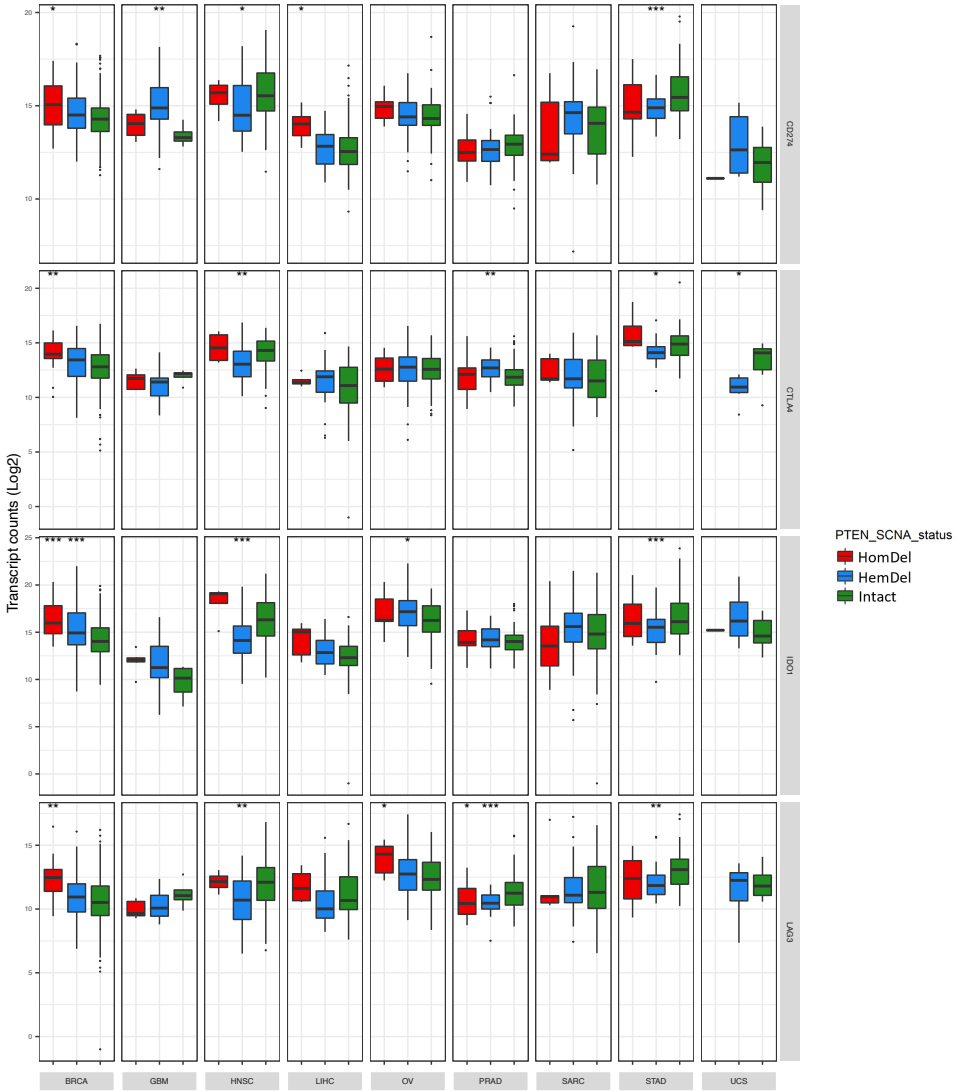

Supplementary figure 9

a

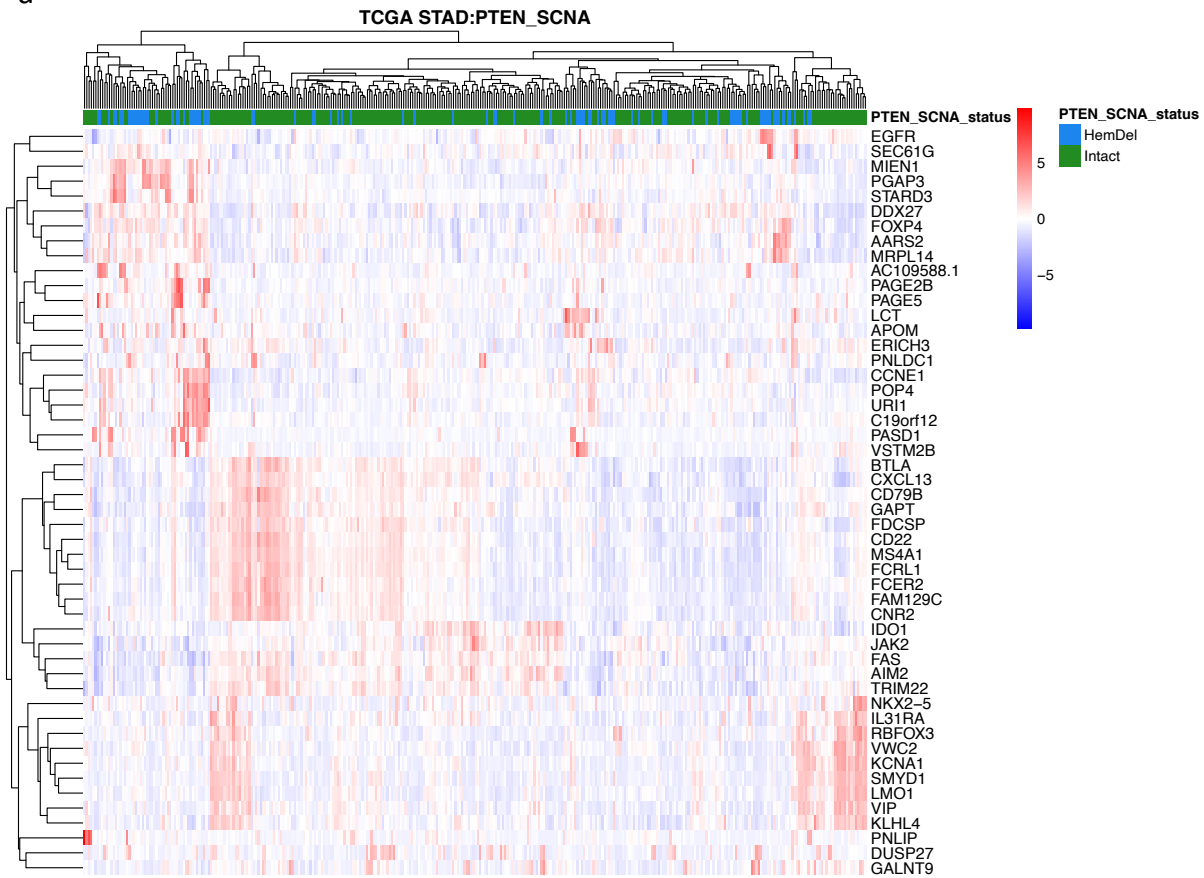

b

ID	Description	qvalue
GO:0000819	sister chromatid segregation	1,75E+06
GO:0000070	mitotic sister chromatid segregation	1,75E+06
GO:0007059	chromosome segregation	2,77E+07
GO:0000280	nuclear division	2,77E+07
GO:0098813	nuclear chromosome segregation	5,81E+06
GO:0051321	meiotic cell cycle	1,05E+12
GO:0016126	sterol biosynthetic process	5,01E+11
GO:0006695	cholesterol biosynthetic process	5,01E+11
GO:1902653	secondary alcohol biosynthetic process	5,01E+11
GO:0034660	ncRNA metabolic process	7,25E+11

c

ID	Description	qvalue
GO:0002250	adaptive immune response	1,55E-22
GO:0051249	regulation of lymphocyte activation	5,34E-12
GO:0042110	T cell activation	7,73E-12
GO:0050778	positive regulation of immune response	9,10E-11
GO:0002443	leukocyte mediated immunity	8,74E-09
GO:0007159	leukocyte cell-cell adhesion	3,17E-07
GO:1903037	regulation of leukocyte cell-cell adhesion	4,46E-07
GO:0050867	positive regulation of cell activation	7,92E-07
GO:0070661	leukocyte proliferation	4,32E-06
GO:0046651	lymphocyte proliferation	1,44E-04

Supplementary figure 10

a

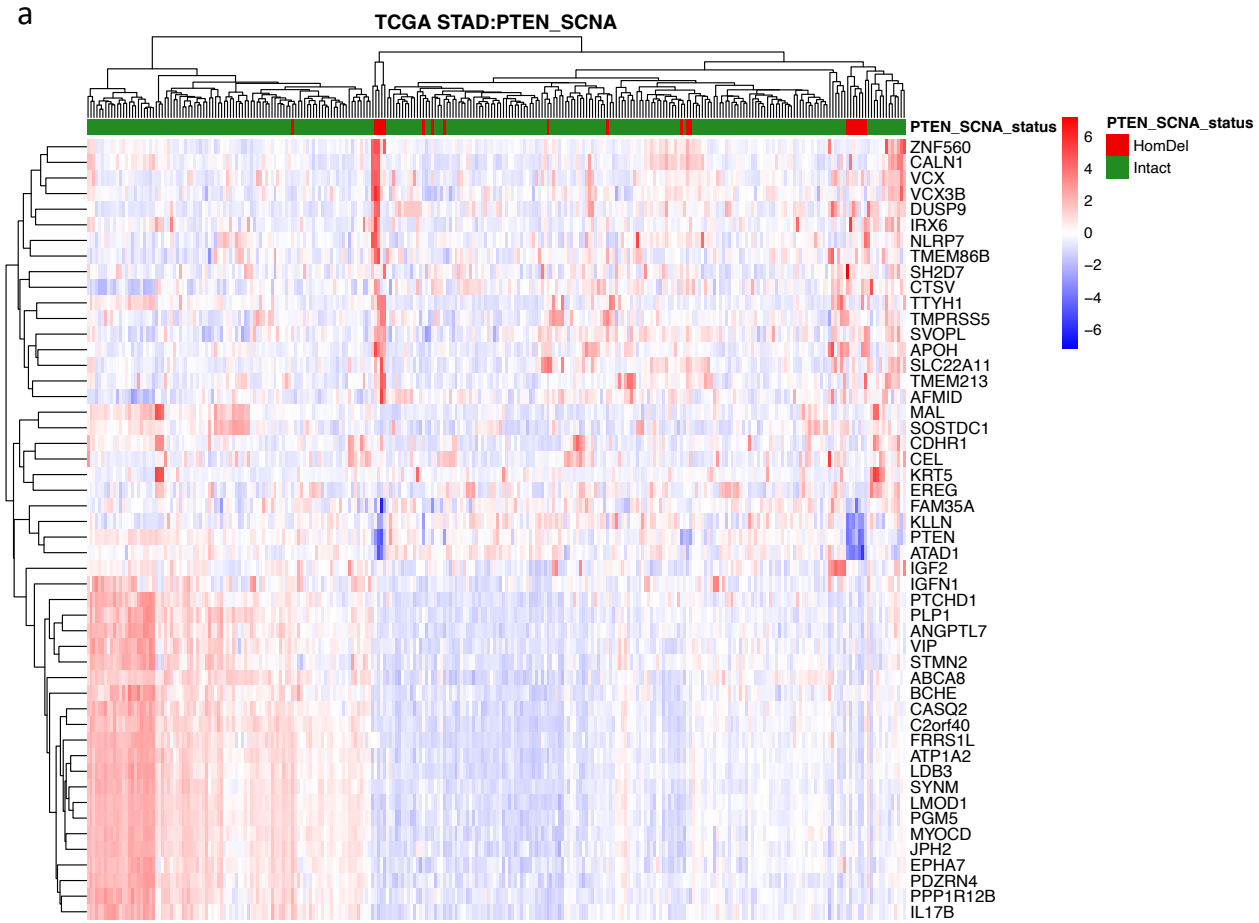

b

ID	Description	qvalue
GO:0003012	muscle system process	5,90E-07
GO:0051480	regulation of cytosolic calcium ion concentration	7,86E+02
GO:0008015	blood circulation	2,35E+04
GO:0010959	regulation of metal ion transport	7,72E+05
GO:0072507	divalent inorganic cation homeostasis	7,96E+05
GO:0008016	regulation of heart contraction	2,15E+08
GO:0042692	muscle cell differentiation	3,11E+07
GO:0060402	calcium ion transport into cytosol	5,62E+08
GO:0034765	regulation of ion transmembrane transport	7,90E+07
GO:0006816	calcium ion transport	1,21E+09

Supplementary figure 11

a

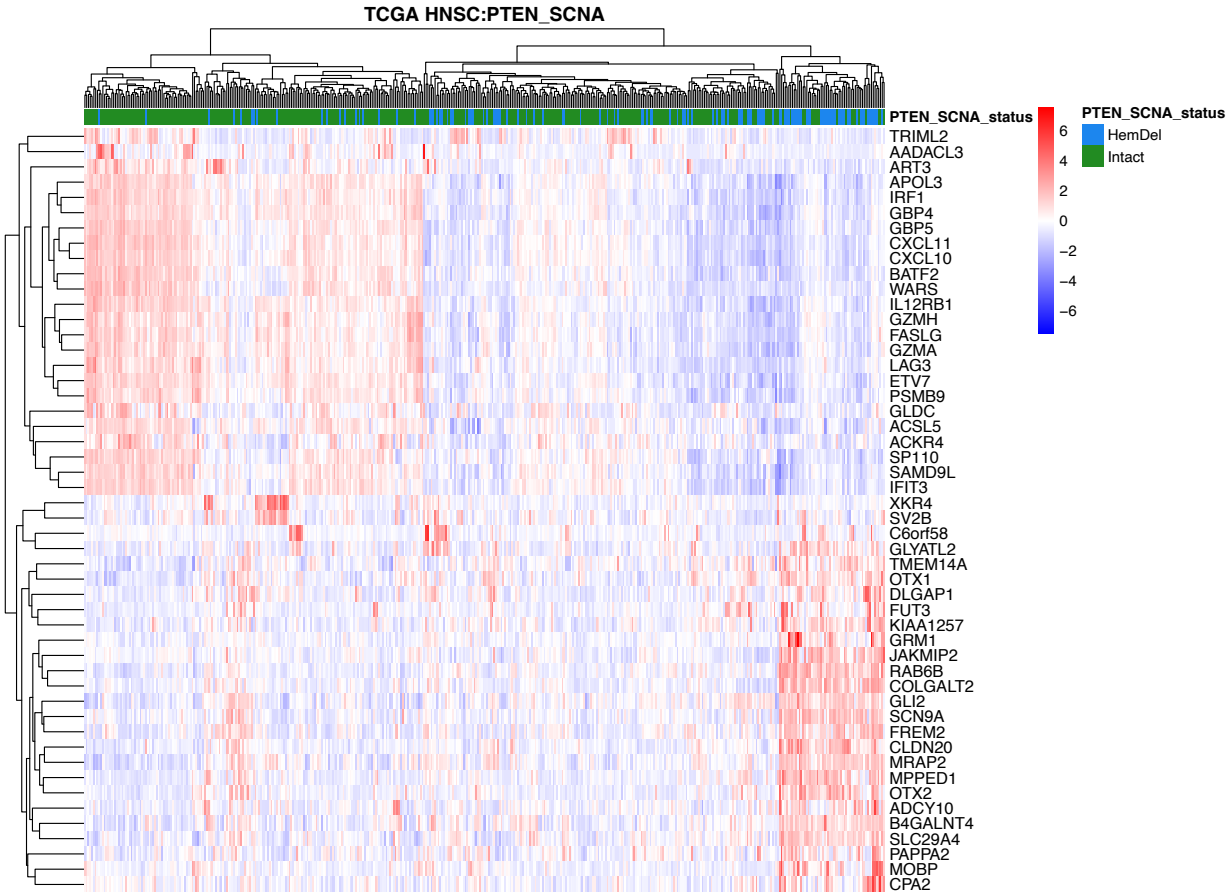

b

ID	Description	qvalue
GO:0050804	modulation of chemical synaptic transmission	0.0012
GO:0099177	regulation of trans-synaptic signaling	0.0012
GO:0009953	dorsal/ventral pattern formation	0.0012
GO:0006749	glutathione metabolic process	0.0029
GO:0007409	axonogenesis	0.0097
GO:0071466	cellular response to xenobiotic stimulus	0.0116
GO:0030900	forebrain development	0.0183
GO:0007224	smoothened signaling pathway	0.0183
GO:0060571	morphogenesis of an epithelial fold	0.0183
GO:0060572	morphogenesis of an epithelial bud	0.0183

c

ID	Description	qvalue
GO:0002250	adaptive immune response	2,90E-53
GO:0002449	lymphocyte mediated immunity	1,34E-27
GO:0050778	positive regulation of immune response	2,30E-27
GO:0042110	T cell activation	2,75E-27
GO:0051249	regulation of lymphocyte activation	4,96E-22
GO:0002697	regulation of immune effector process	9,23E-20
GO:0007159	leukocyte cell-cell adhesion	3,95E-17
GO:0032943	mononuclear cell proliferation	9,05E-17
GO:0001819	positive regulation of cytokine production	1,26E-15
GO:0046651	lymphocyte proliferation	1,38E-15

Supplementary figure 12

a

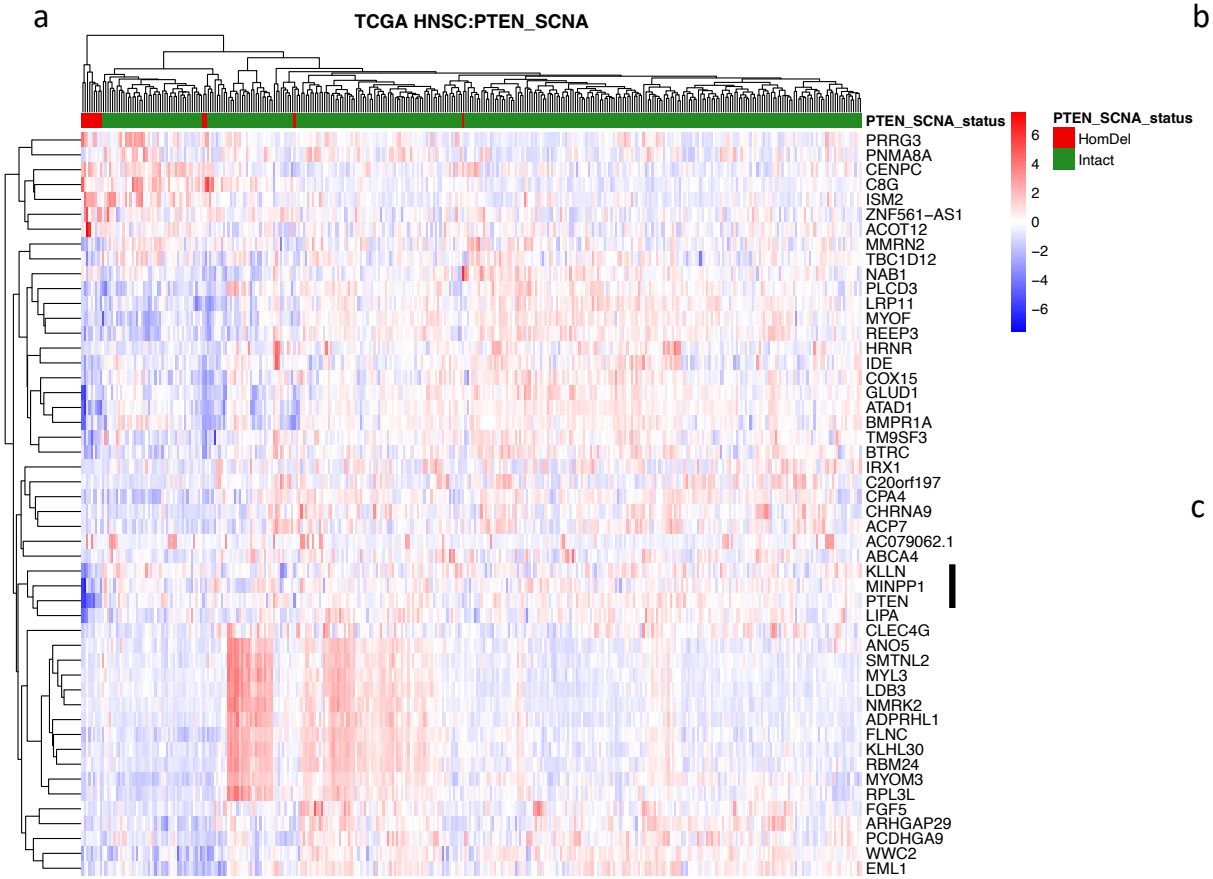

b

ID	Description	qvalue
GO:0006260	DNA replication	8,25E+09
GO:0007059	chromosome segregation	8,25E+09
GO:0051321	meiotic cell cycle	5,49E+09
GO:0098813	nuclear chromosome segregation	1,39E+12
GO:0000280	nuclear division	1,39E+12
GO:0034508	centromere complex assembly	1,92E+11
GO:0006335	DNA replication-dependent nucleosome assembly	0.0023
GO:0034723	DNA replication-dependent nucleosome organization	0.0023
GO:0071824	protein-DNA complex subunit organization	0.0028
GO:0007098	centrosome cycle	0.0028

c

ID	Description	qvalue
GO:0003012	muscle system process	2,71E-09
GO:0055001	muscle cell development	2,11E+00
GO:0014706	striated muscle tissue development	3,43E+01
GO:0030239	myofibril assembly	7,66E+00
GO:0007517	muscle organ development	2,85E+04
GO:0031032	actomyosin structure organization	3,33E+04
GO:0048738	cardiac muscle tissue development	3,80E+04
GO:0050879	multicellular organismal movement	6,46E+04
GO:0050881	musculoskeletal movement	6,46E+04
GO:0008015	blood circulation	3,51E+06

Supplementary figure 13

a

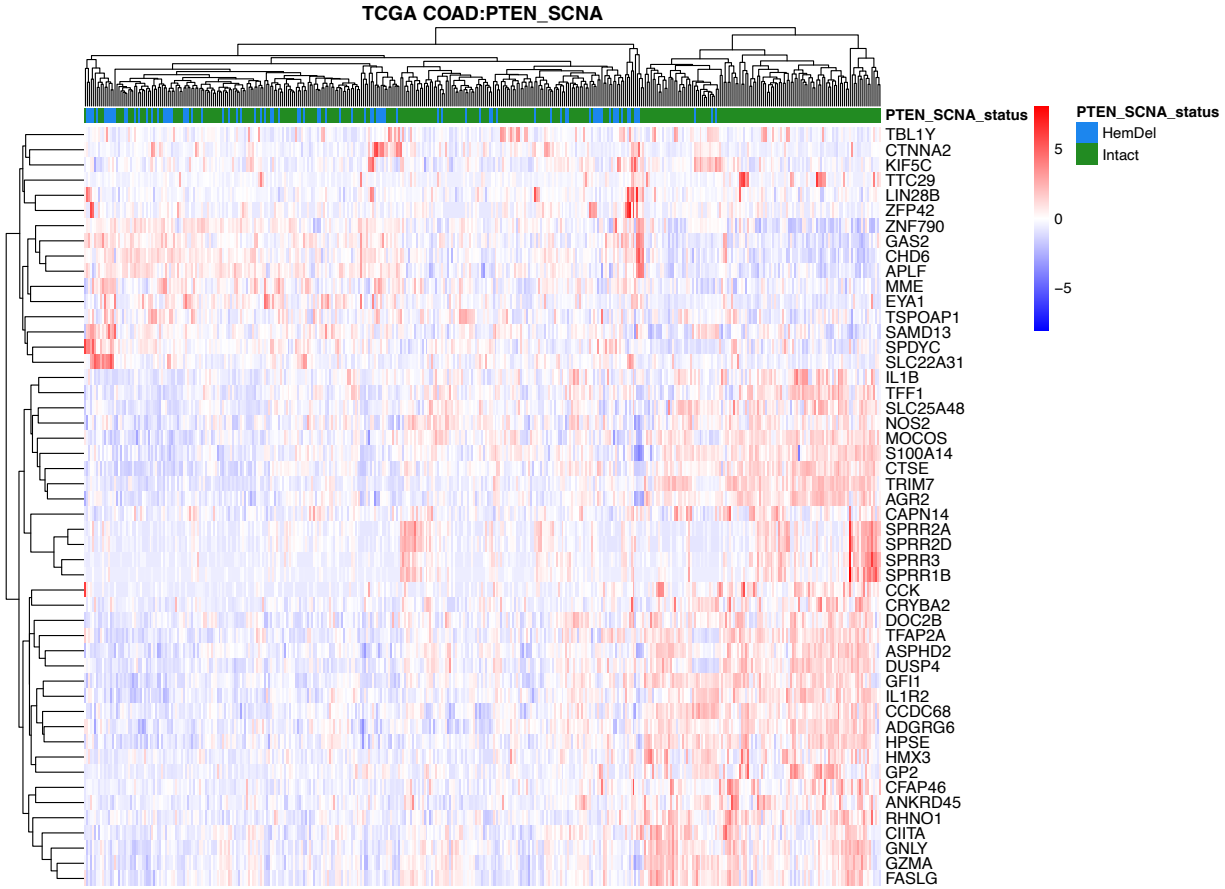

b

ID	Description	qvalue
GO:0034341	response to interferon-gamma	1,93E+10
GO:0002449	lymphocyte mediated immunity	1,93E+10
GO:0002250	adaptive immune response	1,93E+10
GO:0002228	natural killer cell mediated immunity	8,21E+10
GO:0045333	cellular respiration	1,12E+12
GO:0002396	MHC protein complex assembly	2,46E+12
GO:0001906	cell killing	2,49E+12
GO:0009615	response to virus	2,49E+12
GO:0001909	leukocyte mediated cytotoxicity	3,67E+12
GO:0002495	antigen processing and presentation of peptide antigen via MHC class II	3,67E+12

Supplementary figure 14

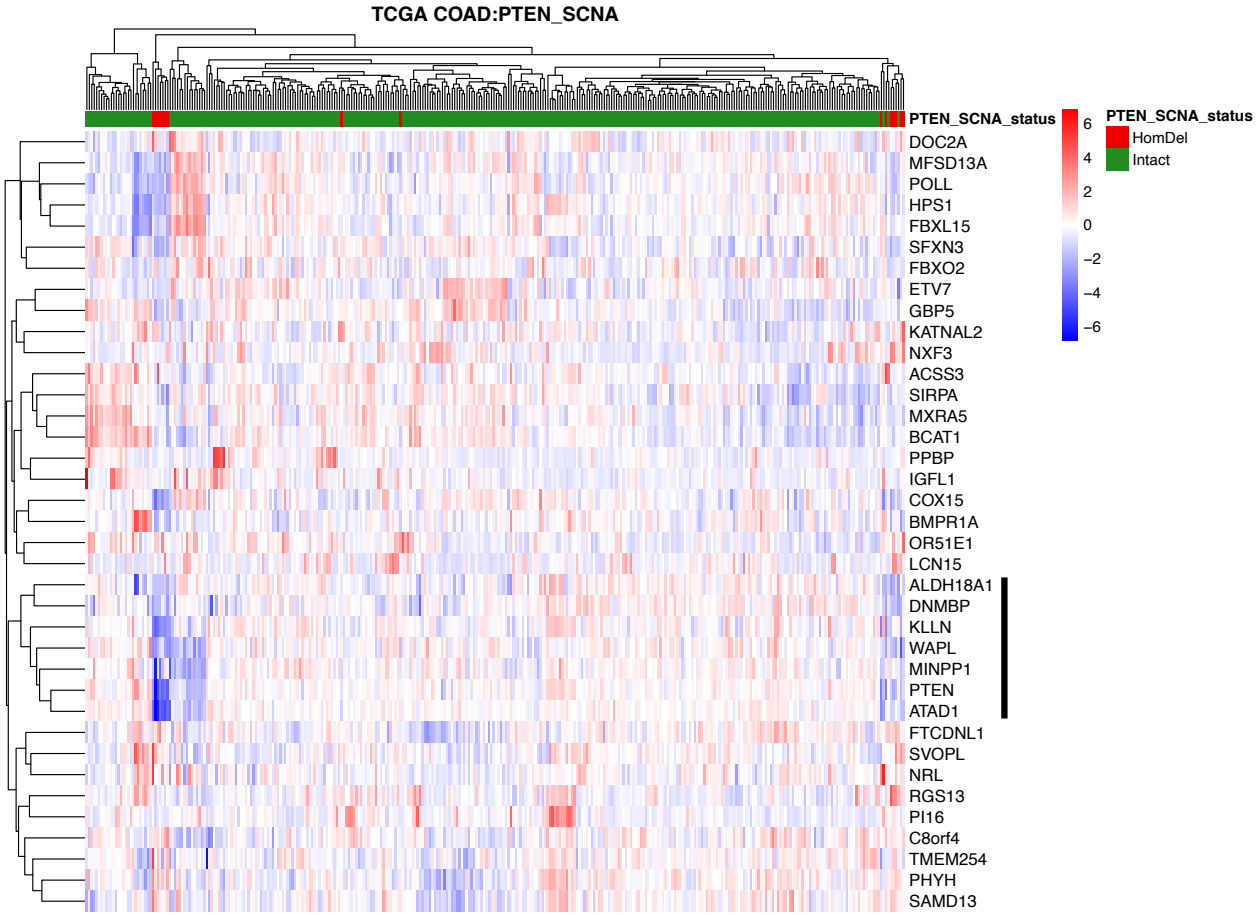

Supplementary figure 15

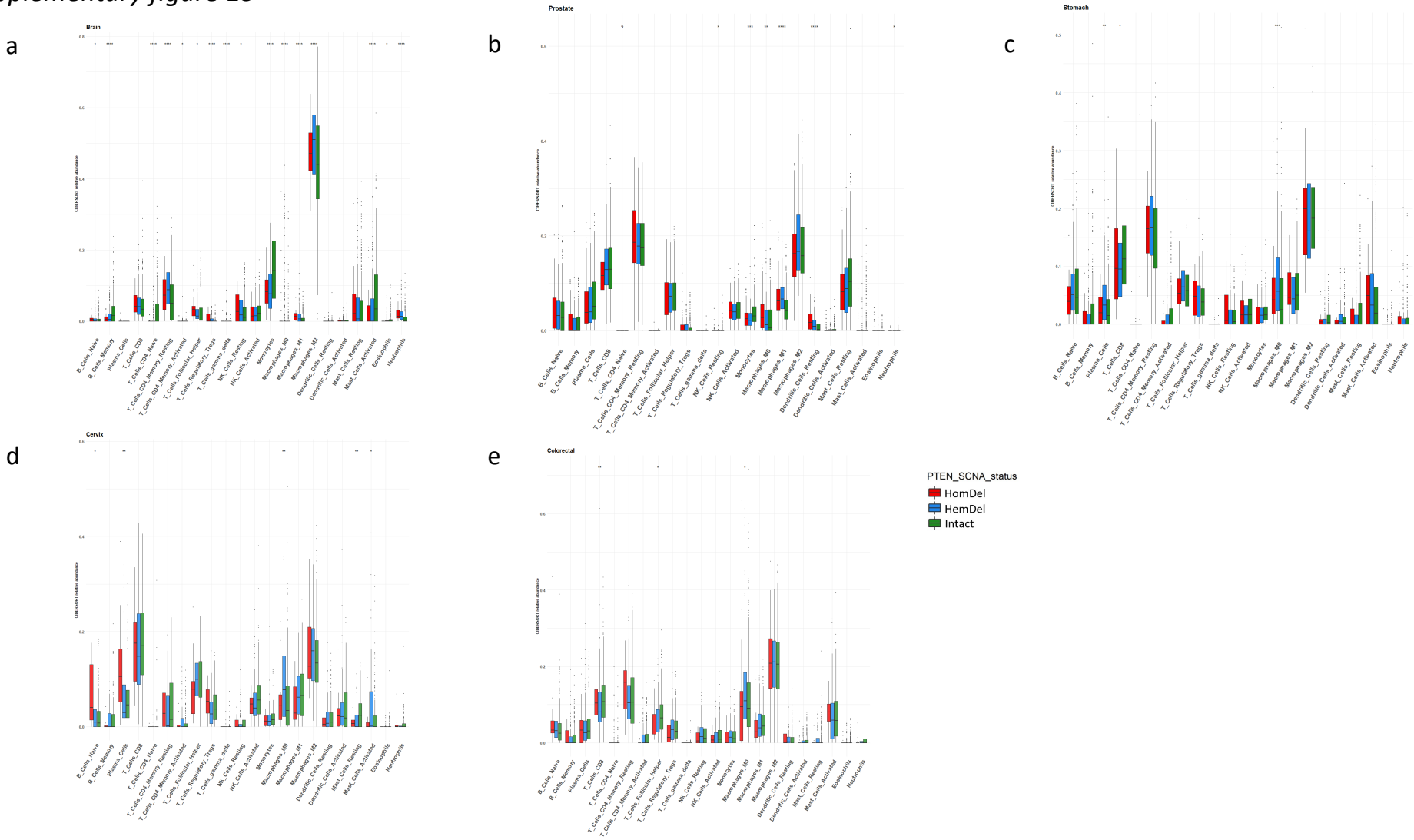
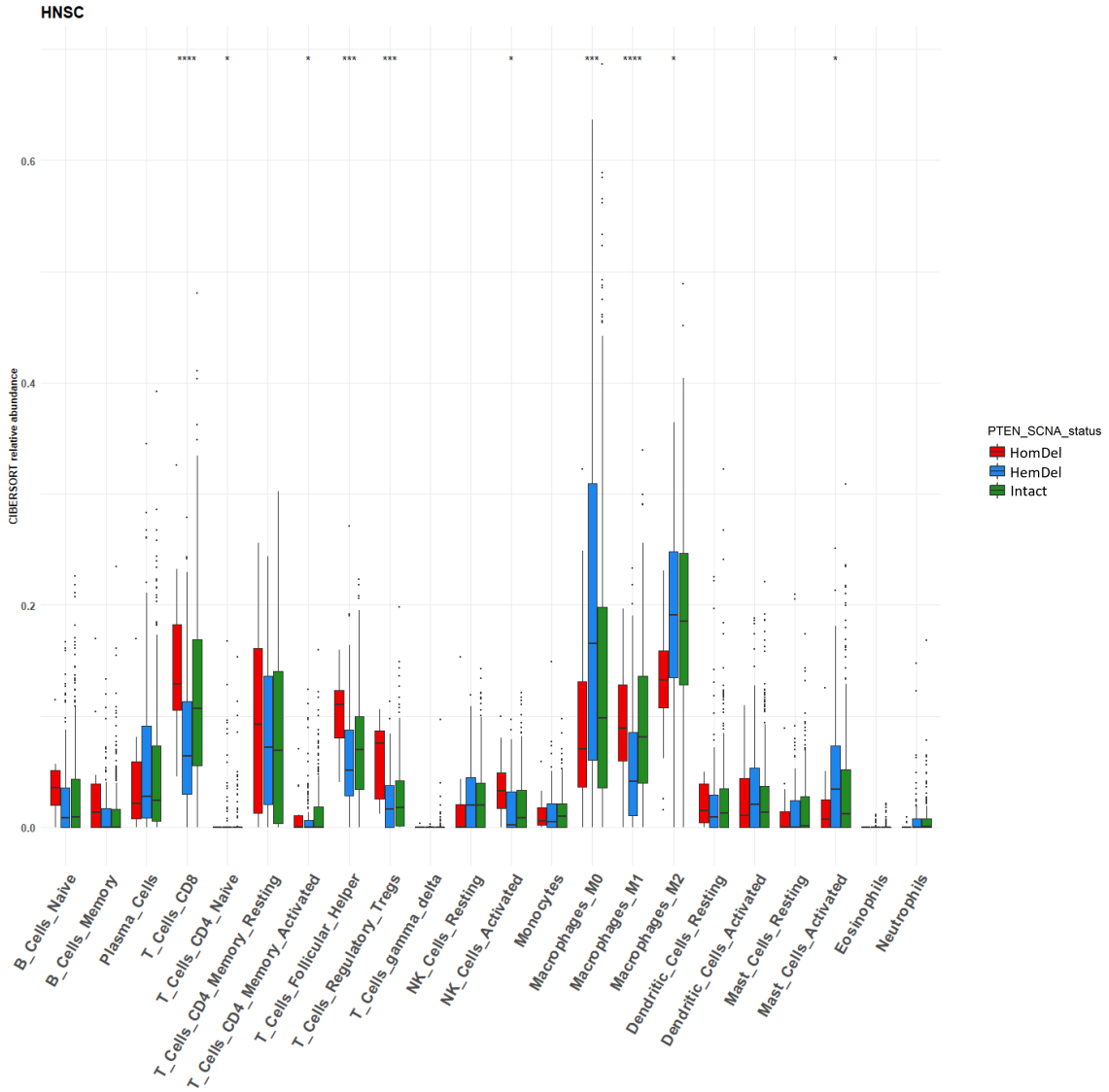
Supplementary figure 16